Comments on Inorganic Chemistry, 00: 1–39, 2018

ISSN: 0260-3594 print / 1548-9574 online
DOI: https://doi.org/10.1080/02603594.2018.1509856

Mechanistic elucidation of Two Catalytically Versatile Iron(II)- and α-Ketoglutarate-Dependent Enzymes: Cases Beyond Hydroxylation

Wei-Chen Chang,[1] Pinghua Liu,[2] and Yisong Guo[3]

[1]Department of Chemistry, North Carolina State University, Raleigh, North Carolina, USA
[2]Department of Chemistry, Boston University, Boston, Massachusetts, USA
[3]Department of Chemistry, Carnegie Mellon University, Pittsburgh, Pennsylvania, USA

Iron(II)- and α-ketoglutarate-dependent (Fe/αKG) enzymes catalyze a large array of biologically important and chemically challenging reactions. Although the mechanism of the hydroxylation reaction catalyzed by these enzymes has been revealed in great detail, the mechanisms of other reactions are still largely unknown. The molecular bases for controlling the diverse reaction outcomes branching from a common reactive intermediate, the ferryl (Fe^{IV} = O) intermediate, are not well understood. By using a combined biochemical, bioorganic, and spectroscopic approach, we have studied the mechanisms of two newly discovered Fe/αKG enzymes, FtmOx1 and AsqJ. The former catalyzes a novel endoperoxidation reaction; the latter catalyzes a consecutive desaturation and epoxidation reaction. Our studies disclose some of the strategies utilized by Fe/αKG enzymes to control reactivity, namely the effect of redox/polar residues near the iron center, the electronic properties of the substrate, and the intrinsic reactivity of the ferryl intermediate.

Address correspondence to Yisong Guo, Department of Chemistry, Carnegie Mellon University, Pittsburgh, PA, USA. E-mail: ysguo@andrew.cmu.edu

Color versions of one or more of the figures in the article can be found online at www.tandfonline.com/gcic.

1. INTRODUCTION

Iron(II)- and α-ketoglutarate (αKG, also known as 2-oxoglutarate)-dependent (Fe/αKG) enzymes constitute a large superfamily of non-heme iron-containing enzymes[1] discovered in microbes, plants, and animals. By using αKG as the co-substrate and molecular oxygen (O_2) as the terminal oxidant, Fe/αKG enzymes catalyze a bewildering array of regio-/stereospecific oxidative transformations, including hydroxylation, halogenation, endoperoxidation, desaturation, epoxidation, ring formation, and ring expansion.[2–6] Some of these transformations are key chemical steps in important biological pathways, such as DNA/RNA repair,[7–11] gene regulation,[12–23] O_2 sensing,[24–27] and natural product biosynthesis.[28,29] In recent years, some members of this family have also been considered as therapeutic targets for a wide range of diseases, including cancer and anemia.[30]

Biochemical studies on Fe/αKG enzymes can be dated back more than a half century. Early studies focused on characterizations of prolyl 4*R*-hydroxylase (P4H), prolyl 3*S*-hydroxylase (P3H), and lysyl 5*R*-hydroxylase (PLOD) that catalyze the stereospecific conversion of proline or lysine side chains to hydroxyproline or hydroxylysine.[31–34] These enzymes are involved in post-translational processing of collagen in mammals.[35] The requirement of Fe (II), αKG, and O_2 for the enzyme activity, the regio- and stereospecific hydroxylation site with the replacement of hydrogen atom on that site, the source of hydroxyl oxygen, as well as the production of equimolar quantities of hydroxylated product, succinate, and CO_2 were established by various biochemical activity assays with isotope labeled chemicals ([4-^{3}H]proline, [1-^{14}C] αKG, and $^{18}O_2$). These studies have defined the overall hydroxylation reaction of Fe/αKG enzyme (Scheme 1). These early studies also identified ascorbic acid as an important reagent to enhance the enzyme activity; however, it was not directly involved in enzyme catalysis, but was viewed as a reducing reagent to reactivate the enzyme in multiple turn-over reactions, and likely to prevent iron from oxidizing to the ferric form.[35] Over the years, the Fe(II)-, αKG-, and O_2-dependent hydroxylase reactivity has been further explored in other Fe/αKG enzymes discovered in many different biological pathways. Some

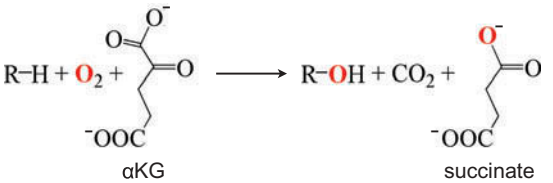

Scheme 1: The overall reaction of Fe/αKG enzyme-catalyzed hydroxylation. R-H stands for the C-H bond being activated during the reaction.

examples are listed in the following. In fatty acid metabolism, two Fe/αKG-dependent hydroxylases, 6-N-trimethyllysine and γ-butyrobetaine hydroxylases, have been identified in L-carnitine biosynthesis.[36–39] In free amino acid modification, many Fe/αKG-dependent hydroxylases have been identified to produce hydroxylated amino acids with high regio-specificity; some of these products are further incorporated into antibiotics.[40] In pyrimidine metabolism, thymine 7-hydroxylase (T7H), one of the first characterized Fe/αKG-dependent enzymes, catalyzes three sequential hydroxylation reactions on the methyl group of thymine, converting it to 5-carboxyuracil.[41–44] In sulfonate and sulfate metabolism, taurine dioxygenase (TauD) catalyzes hydroxylation of taurine, which spontaneously decomposes to aminoacetaldehyde and sulfite.[45,46] In the hypoxia signaling pathway, P4Hs are responsible for the modifications of the α-subunit of the hypoxia-inducible factor (HIF-1) in humans; HIF-1 is the key component in the hypoxia signaling pathway.[24,25] Another commonly observed reaction catalyzed by Fe/αKG enzymes is demethylation, which can be viewed as hydroxylation on the methyl group of the substrate followed by the spontaneous loss of formaldehyde. Fe/αKG-dependent demethylases have been found in gene regulation pathways, such as histone demethylation catalyzed by Fe/αKG enzyme JmjC,[12–15,17] and in repairing DNA/RNA, such as demethylation of alkylated DNA/RNA by the AlkB enzyme family.[7,8,11,47] Recently, more evidence suggests that Fe/αKG-dependent demethylation on DNA/RNA may contribute to epigenetic regulation by controlling the methylation status of DNA/RNA.[20] All of these discoveries confirm the ubiquity and importance of Fe/αKG- and O_2-dependent hydroxylase reactivity in many fundamental biological processes.

Although hydroxylation is the most common reactivity exhibited by the Fe/αKG enzyme family, other reactivities have also been discovered (Scheme 2). Three well-characterized members of the Fe/αKG enzyme family that exhibit interesting non-hydroxylation reactivity are deacetoxycephalosporin C synthase/deacetylcephalosporin C synthase (DAOCS/DACS), clavaminate synthase (CAS),[48–51] and carbapenem synthase (CarC).[52,53] They are all multifunctional enzymes involved in β-lactam antibiotic biosynthesis. DAOCS/DACS catalyzes a consecutive reaction, including an unprecedented oxidative ring expansion of the penam ring of penicillin N (penN) to the cephem moiety of deacetoxycephalosporin C (DAOC), and further hydroxylation on the terminal methyl group on the C_3 of DAOC to form deacetylcephalosporin C (DAC). Interestingly, in bacteria such as *S. clavuligerus*, the conversions from penN to DAOC, and DAOC to DAC, are catalyzed by two separate but highly similar Fe/αKG enzymes, while in fungi such as *C. acremonium*, a single enzyme catalyzes all of the reactions. CAS is a remarkable tri-functional enzyme in the pathway of clavulanic acid biosynthesis found in *S. clavuligerus*. This enzyme catalyzes hydroxylation reaction followed by cyclization and desaturation reactions. Finally, CarC found in *P. carotovorum*

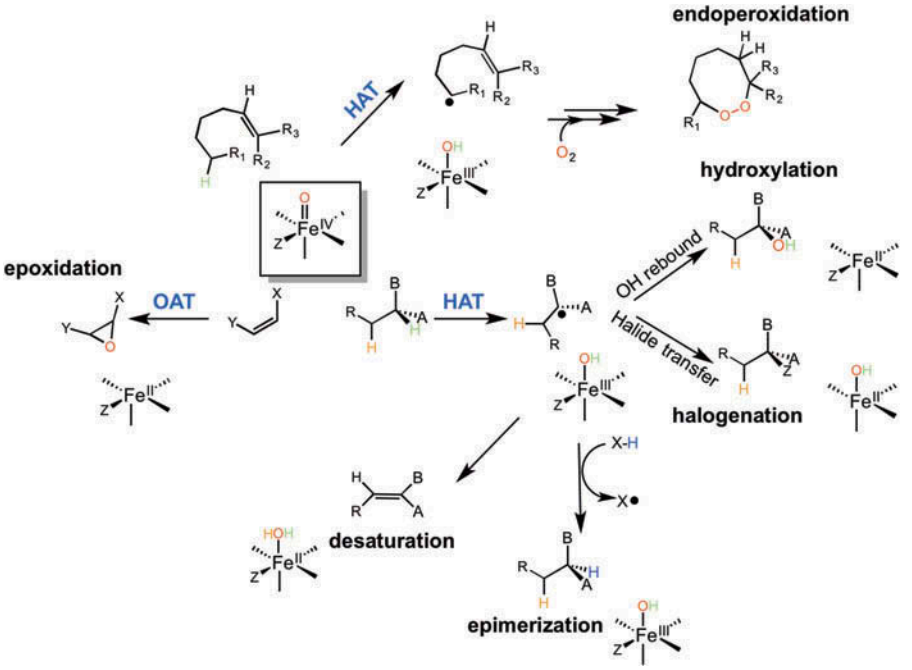

Scheme 2: Diverse catalytic activities exhibited by Fe/αKG-dependent enzymes. HAT refers to hydrogen atom transfer; OAT refers to oxygen atom transfer.

catalyzes two sequential non-hydroxylation reactions: a unique redox neutral epimerization to convert (3*S*,5*S*)-carbapenam to (3*S*,5*R*)-carbapenam, and further desaturation to yield (5*R*)-carbapenem-3-carboxylate. More non-hydroxylation reactivities have been identified in Fe/αKG enzymes in recent years, such as epoxidation catalyzed by hyoscyamine 6β-hydroxylase (H6H) in the biosynthesis of scopolamine,[54–57] an alkaloid produced by *H. niger*; halogenation catalyzed by SyrB2[58,59] in the biosynthesis of syringomycin E, a phytotoxin generated by *P. syringae*, and CytC3[60,61] in cytotrienin biosynthesis from *Streptomyces* sp.; endoperoxidation catalyzed by FtmOx1 in the biosynthesis of verruculogen,[62,63] a mycotoxin produced by *A. fumigatus*; and an unprecedented C(sp2)-C(sp3) bond formation catalyzed by 2-ODD in the biosynthesis of podophyllotoxin,[64] a natural product precursor of the chemotherapeutic etoposide in *P. hexandrum*. Thus, all of these studies not only establish the catalytic diversity of Fe/αKG enzymes, they also raise a fundamental mechanistic question on how these diverse reactivities are controlled by this family of enzymes.

Early mechanistic understandings of the Fe/αKG enzyme-catalyzed hydroxylation reaction were largely obtained from steady-state kinetic studies on P4Hs. Based on these studies, Hanauske-Abel and Günzler, in 1982, put

forward a general mechanism of the hydroxylation reaction catalyzed by Fe/αKG enzymes, where a ferryl intermediate as the key reactive species was proposed for the first time.[65] The experimental validation of this intermediate came more than 20 years later from the seminal work from Bollinger, Krebs, and coworkers by using transient enzyme kinetics and spectroscopic tools.[66,67] At the same time, molecular-level understandings of Fe/αKG enzymes were greatly enhanced from the high-resolution crystal structures of several Fe/αKG enzymes that appeared in the late 1990s and early 2000s.[68–72] These structures revealed a common protein fold, a double-stranded β-helix (DSBH), cupin, or jelly-roll, for Fe/αKG enzymes and related non-heme iron enzymes, and a highly conserved iron-binding site consisting of a His-X-Asp/Glu...His (HXD/E...H) moiety, termed the 2-His-1-carboxylate facial triad.[73] It was further suggested that three water molecules occupy three iron-binding sites in the resting state of enzyme to give a pseudo-octahedral geometry of the iron center. For all of the structurally and spectroscopically characterized Fe/αKG enzymes, αKG forms a bidentate binding to the iron center by replacing two of the three water molecules, and the primary substrate binds in the vicinity of the iron center (an exception is ethylene-forming enzyme (EFE), where in one of the reported crystal structures a mono-dentate binding of αKG is proposed[74]). Model chemistry studies on mimicking the structures of the ferrous and the ferryl state of enzymes also greatly enhanced our understanding of Fe/αKG enzymes.[5,75] Furthermore, all of these experimental efforts were joined by computational studies; in particular, density functional theory (DFT) calculations[76–79] and, more recently, large-scale quantum mechanics/molecular mechanics (QM/MM) calculations,[80–83] to elucidate the fundamental structural/function relationship of Fe/αKG enzymes.

In this review, we will first briefly summarize the current mechanistic understandings of Fe/αKG enzymes and the major questions that remain to be solved in understanding the catalytic diversity of this enzyme family. Secondly, we will describe our recent results on the mechanistic elucidation of two newly discovered Fe/αKG enzymes, FtmOx1 and AsqJ, by using a multifaceted approach, including organic synthesis, structural determination, transient kinetics, and advanced spectroscopic methods. The implications of these results in improving our understanding of Fe/αKG enzymes will also be discussed.

2. IRON CENTER STRUCTURE AND GENERAL MECHANISM OF FE/αKG ENZYMES

The resting state of Fe/αKG enzymes contains a mononuclear ferrous (Fe(II)) center, which is ligated by a conserved 2-His-1-carboxylate facial triad, thus

creating three open coordination sites for the Fe(II) center (Figure 1). This structurally conserved active center was first revealed in the crystal structure of isopenicillin N synthase (IPNS), a mononuclear nonheme iron enzyme related to Fe/αKG enzymes, yet not requiring αKG as the co-substrate.[68,84,85] Later crystallographic studies revealed similar active center structural motifs in Fe/αKG enzymes, such as in DAOCS[69] and TauD.[71] Exceptions to this conserved 2-His-1-carboxylate facial triad are those found in αKG-dependent halogenases, where the iron-ligated carboxylate group is replaced with halides.[86–88] These crystal structures further illustrated that, in the absence of αKG and the primary substrate of the enzymes, the open coordination sites of the Fe(II) center are generally occupied by water molecules (Figure 1). The crystallographic results were confirmed by spectroscopic studies. By using circular dichroism (CD) and magnetic circular dichroism (MCD),[89] Solomon and coworkers studied the Fe(II) center in CAS[50,51] and TauD.[90] Two d-d transitions in the near-IR region with positive MCD bands were observed with an energy splitting of $\Delta^5E_g \sim 2000\ cm^{-1}$, which is indicative of a distorted six-coordinated high-spin ($S = 2$) Fe(II) center (Figure 1).

The co-substrate αKG directly binds to the Fe(II) center in a bi-dentate fashion through the C_2-carbonyl oxygen and one of its C_1 carboxylate oxygens, resulting in the replacement of two coordinated water molecules (Figure 1). This binding mode was first revealed through MCD studies on CAS,[50] and then confirmed by the crystallographic data on other Fe/αKG enzymes. This enzyme-Fe(II)-αKG ternary complex retains a six-coordinated geometry with one water molecule still coordinating with the Fe(II). Another spectroscopic feature of this ternary complex is a weak metal-to-ligand charge transfer (MLCT) band observed at ~ 520 nm with an extinction coefficient of ~ 200 $M^{-1}\ cm^{-1}$, which gives a pink/purple color to the enzyme-Fe(II)-αKG ternary complex in Fe/αKG enzymes (Figure 1).[50,91] This MLCT band has been assigned as the transitions between d orbitals of Fe (d_{yz}, d_{z2} and d_{x2-y2}) and the π* of the α-keto carboxylate moiety of αKG.[50] Hausinger and co-workers,[91] as well as other research groups, have utilized this MLCT band to determine the binding affinities of Fe(II), αKG, and the primary substrate in Fe/αKG enzymes. Although the αKG binding mode to the Fe(II) center is almost exclusively bi-dentate with the C_2-carbonyl oxygen invariantly *trans* to the carboxylate of the 2-His-1-carboxylate facial triad, the position of the C_1 carboxylate of αKG adopts two orientations revealed by the reported crystallographic data of various Fe/αKG enzymes.[92] In one orientation, the C_1 carboxylate group is located *trans* to the proximal (closer to N-terminus of the protein) histidine of the 2-His-1-carboxylate facial triad (the in-line configuration). In the other orientation, the C_1 carboxylate group is located *trans* to the distal histidine (the off-line configuration) (Figure 1). The mechanistic implication of these two distinct configurations is still not fully understood. Furthermore, a mono-dentate binding of αKG to the Fe(II) center was recently

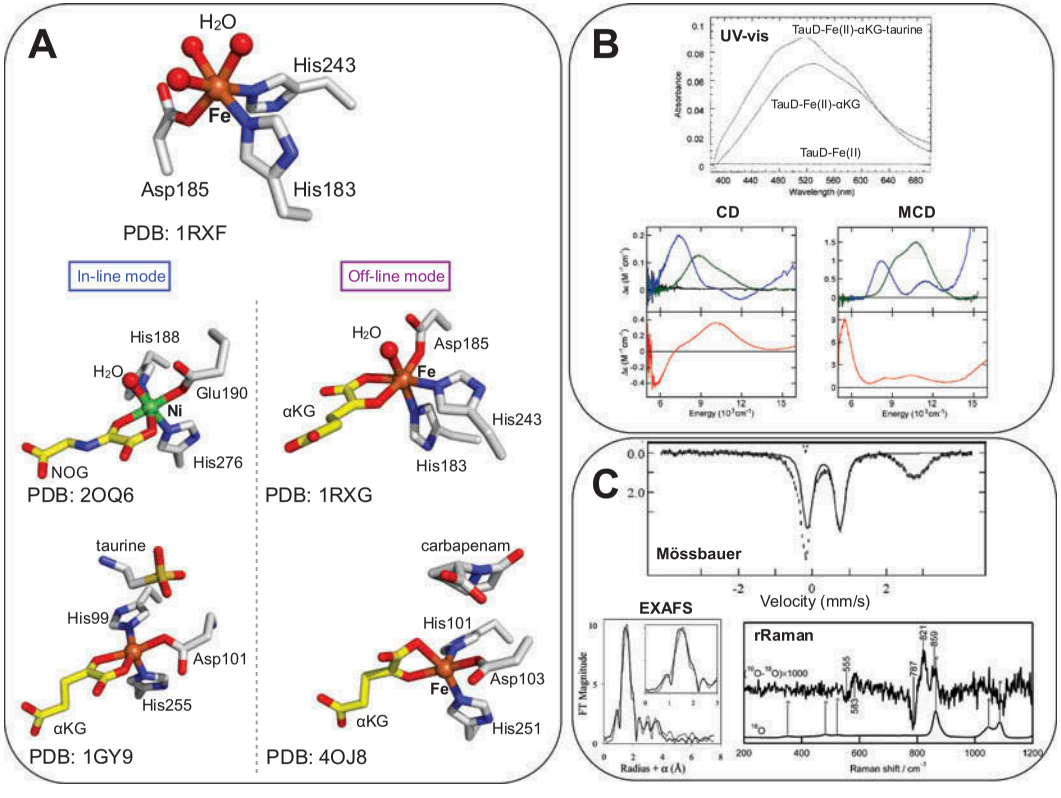

Figure 1: Iron center structures and the related spectroscopic features. Panel A: Iron center structures with and without αKG (or enzyme inhibitor, NOG) and primary substrate binding as well as in-line and off-line binding mode of αKG. Panel B: Selected spectroscopic features of Fe(II) only, Fe(II)-αKG complex, and Fe(II)-αKG-substrate complex. Reproduced with permission from Refs. 90 and 91. © 1999 and 2007, American Chemical Society. Permission to reuse must be obtained from the rightsholder. Panel C: Selected spectroscopic features of the ferryl intermediate. Reproduced with permission from Refs. 66, 105 and 106. © 2003 and 2004, American Chemical Society. Permission to reuse must be obtained from the rightsholder.

observed in one of the reported crystal structures of the enzyme-Fe(II)-αKG ternary complex of EFE enzyme,[74] which leads to the dramatically decreased MLCT optical band in the EFE-Fe(II)-αKG ternary complex.[93,94] This is the only known exception to the otherwise conserved bi-dentate αKG-binding mode to the Fe(II) center of Fe/αKG enzymes.

The formation of the reaction complex in Fe/αKG enzymes is completed by the binding of the primary substrate, which is located in the vicinity of the Fe (II) center and stabilized through various hydrophobic or hydrophilic interactions provided by the surrounding protein residues. MCD studies[51,90] on CAS, TauD, and αKG-dependent halogenases revealed that the binding of the primary substrate facilitates the conversion of the six-coordinated Fe(II) center to a five-coordinated one through the elimination of the water molecule (or the weakening of the water binding) in the enzyme-Fe(II)-αKG ternary complex (Figure 1). Mössbauer analyses on the Fe(II) state of TauD were also consistent with the MCD results.[66,67] In going from the TauD-Fe(II) binary complex to the TauD-Fe(II)-αKG-taurine quaternary complex, decreases in the isomer shift (from 1.27 mm/s to 1.16 mm/s) and the quadrupole splitting (from 3.06 mm/s to 2.76 mm/s) were observed, indicating a conversion from a six-coordinated Fe(II) center to a five-coordinated center. The primary substrate binding also causes a subtle blue shift with an increase of the extinction coefficient of the MLCT band at ~ 520 nm. Using this behavior, Hausinger and coworkers determined the binding affinity of taurine, the primary substrate, to TauD.[91] This iron center structural change is further proposed to promote rapid O_2 addition at the onset of Fe/αKG enzyme catalysis, which is supported by transient kinetic studies. For example, in the case of TauD, the binding of taurine activates the Fe(II) center for reaction with O_2 by 1000-fold.[67,95] This substrate-triggered O_2 addition is thought to serve as a protection mechanism to prevent unwanted O_2 activation in order to avoid enzyme self-oxidation.

The general mechanism of the hydroxylation reaction (Scheme 3) catalyzed by Fe/αKG enzymes, proposed initially by Hanauske-Abel and Günzler in 1982, predicts that the addition of O_2 to the reaction complex (enzyme-Fe (II)-αKG-substrate, or the quaternary complex) leads to formation of an Fe (III)-superoxo intermediate, followed by an Fe(IV)-peroxo bicyclic intermediate.[65] The decay of the latter intermediate (Scheme 3, pathway I) through the simultaneous O-O bond cleavage and the conversion of αKG to succinate by decarboxylation affords formation of an unprecedented ferryl (Fe^{IV} = O) intermediate. Alternatively, the decay of the Fe(III)-superoxo intermediate leads to the formation of a Fe(II)-peroxysuccinate intermediate,[96–99] and the subsequent O-O bond cleavage results in the same ferryl species (Scheme 3, pathway II). The existence of the ferryl intermediate was validated by the seminal work from Bollinger, Krebs, and coworkers on studies of the TauD enzyme in 2003.[66] Since then, this intermediate has been observed in a

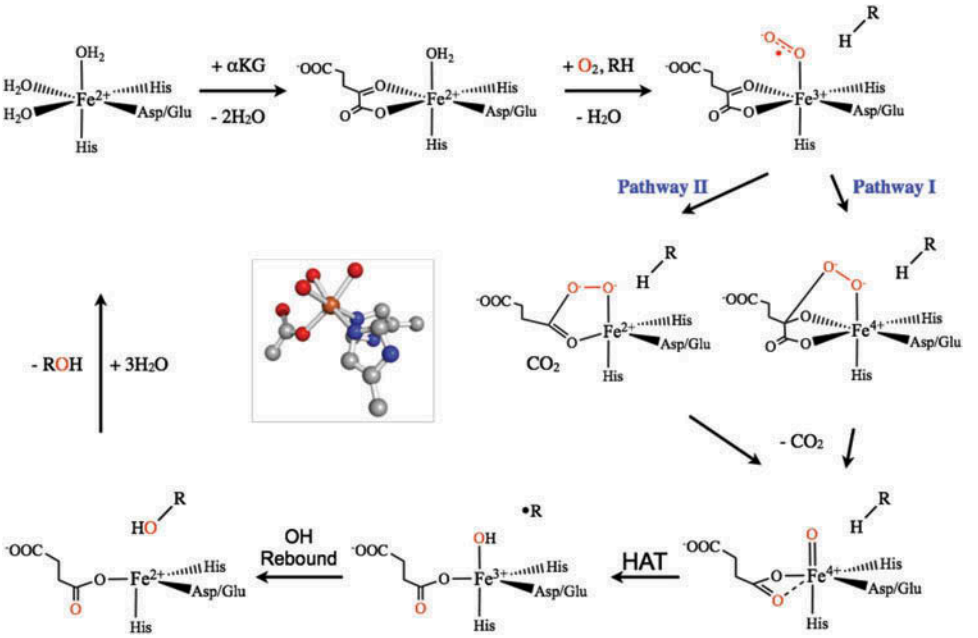

Scheme 3: Generally accepted mechanism of the Fe/αKG enzyme-catalyzed hydroxylation reaction.

dozen of Fe/αKG and related enzymes, confirming that it is the conserved reactive intermediate in the Fe/αKG enzyme catalysis. Due to the highly reactive nature of the ferryl intermediate, its detection relies on the application of spectroscopic tools coupled with the freeze quench technique. The frequently used spectroscopic technique is Mössbauer spectroscopy. All of the reported ferryl intermediates have similar isomer shift (δ = 0.22 – 0.32 mm/s) and quadrupole splitting (ΔE_Q = 0.7 – 1.1 mm/s)[53,59,61,66,100–104] (Figure 1). These Mössbauer parameters confirmed the oxidation state of the ferryl intermediate to be Fe^{4+}. The high-field Mössbauer studies also revealed that the ferryl intermediate has a high-spin (S = 2) ground electronic state. Extended X-ray absorption fine structure (EXAFS) spectroscopy revealed a short Fe-oxo bond (~ 1.60–1.65 Å) in the ferryl species[59,104,105] (Figure 1), which was confirmed by resonance Raman study showing the Fe-oxo stretching frequency at ~ 825 cm^{-1}[106,107] (Figure 1). However, the detailed structure of the ferryl intermediate is still not available. By using nuclear resonance vibrational spectroscopy (NRVS), Solomon and coworkers studied vibrational features of the ferryl intermediate of SyrB2, an αKG-dependent halogenase, and suggested that the SyrB2 ferryl intermediate is most likely five-coordinated.[108] However, a detailed study combining spectroscopic data

with density functional calculations (DFT) suggested that both six- and five-coordinated geometries are possible for the TauD ferryl intermediate.[109]

The decay of the ferryl intermediate, in most cases (Fe/αKG enzyme catalyzed epoxidation is an exception, see section 4), goes through a C-H activation pathway where the Fe(IV) = O moiety abstracts a hydrogen atom (hydrogen atom transfer, HAT) from the targeted C-H bond of the primary substrate to generate a ferric-hydroxo intermediate and a substrate radical. The first direct evidence showing that the ferryl intermediate is responsible for the C-H activation came from the demonstration of a hydrogen/deuterium kinetic isotope effect (H/D KIE) on the decay kinetics of the ferryl intermediate in TauD.[110] A H/D KIE of ~ 50 was observed when the designated hydrogen atom was replaced by a deuterium, such as C_1-$^2H_2$-taurine. Until now, H/D KIEs up to 80 have been observed in various Fe/αKG enzymes.[111] Such a high H/D KIE value suggests that the C-H activation step by the ferryl intermediate consists of a significant hydrogen atom tunneling contribution. By utilizing substrate analogs with different C-H bond strength, ranging from 94 to 106 kcal/mol, Bollinger, Krebs, and coworkers systematically studied the ferryl reactivity in SyrB2, and revealed that the ferryl intermediate in SyrB2 is capable of activating a C-H bond with bond dissociation energy up to 100 kcal/mol.[59]

So far, there is very limited information regarding the detailed electronic and geometric structures of the ferric-hydroxo intermediate after the decay of the ferryl intermediate, and the resulting substrate radical. For all of the characterized αKG-dependent hydroxylases and halogenases, such an intermediate is simply unattainable due to its fleeting nature. For non-hydroxylation reactions, there are two examples where this type of intermediate does accumulate. One is from CarC catalyzed stereoinversion[53]; the other is from FtmOx1 catalyzed endoperoxdation (see section 3 for details). It is generally accepted that the completion of the hydroxylation reaction is accomplished by the formation of a C-O bond between the hydroxyl group from the ferric-hydroxo intermediate and the substrate radical through a "OH-rebound" pathway that was first proposed in cytochrome P450-dependent iron enzymes.[112] Alternatively, in the halogenation reaction, the iron bound halide group rebounds to the substrate radical instead of the OH group. Finally, the release of the enzyme product and the regeneration of the enzyme quaternary complex have been studied in detail in TauD, where the overall rate-limiting step of Fe/αKG enzyme catalysis likely is the product release, which is followed by a rapid and ordered binding of αKG and then the primary enzyme substrate to regenerate the enzyme-Fe(II)-αKG-substrate complex.[46,91]

Although the general reaction mechanism—in particular, for the hydroxylation reaction—along with the iron center structures in the ferrous state of several Fe/αKG enzymes have been studied in great detail, major questions still remain to be solved to improve fundamental understandings of Fe/αKG

enzymes, which include (1) what are the molecular bases that are used to precisely control the diverse reactivity outcomes; and (2) what are the detailed mechanisms of Fe/αKG enzymes that catalyze novel but non-hydroxylation reactions. By using a multifaceted approach, including mechanistic probe design, structural determination, transient kinetics, and advanced spectroscopic methods, we have studied two newly discovered Fe/αKG enzymes, FtmOx1 and AsqJ. These studies enrich our understanding of Fe/αKG catalysis, and provide insights to start unraveling the strategies that Fe/αKG enzymes utilize to precisely control the reaction outcomes.

3. ELUCIDATION OF ENDOPEROXIDE BOND FORMATION BY FTMOX1

Endoperoxide-containing natural products,[113] isolated mainly from plants, fungi, and marine organisms, exhibit a wide spectrum of pharmacological activities, including antimicrobial, antibacterial, and anticancer activities.-[114–116] For example, artemisinin, one of the notable endoperoxide-containing natural products isolated from *Artemisia annua*, possesses the most rapid action of all current drugs against the multidrug-resistant *Plasmodium falciparum* responsible for malaria (Scheme 4). Although the exact mode of action

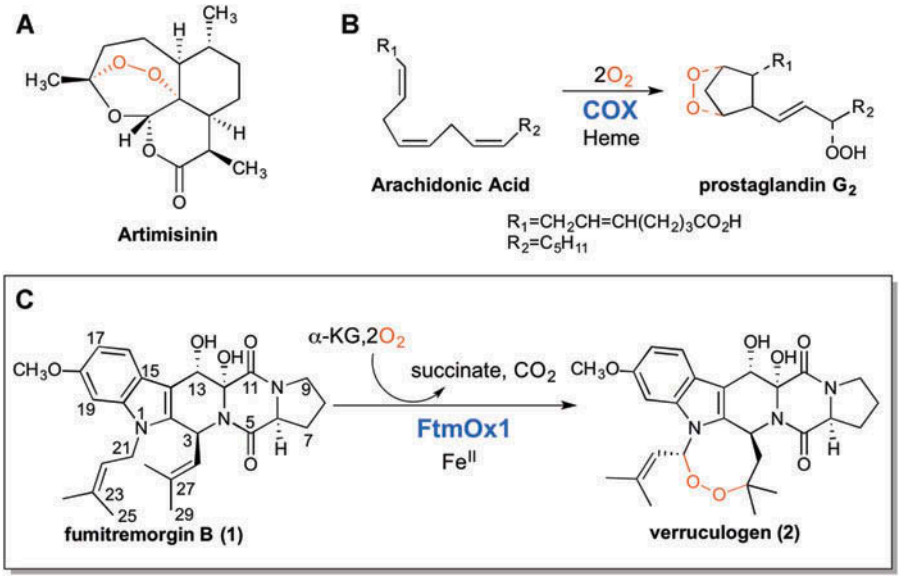

Scheme 4: (A) The molecular structure of artimisinin; and the endoperoxidation reaction catalyzed by prostaglandin H synthase (COX) (B) and by FtmOx1 (C). The endoperoxide functional groups are highlighted in red. The reaction stochiometry of the FtmOx1 reaction is derived from single turnover conditions.

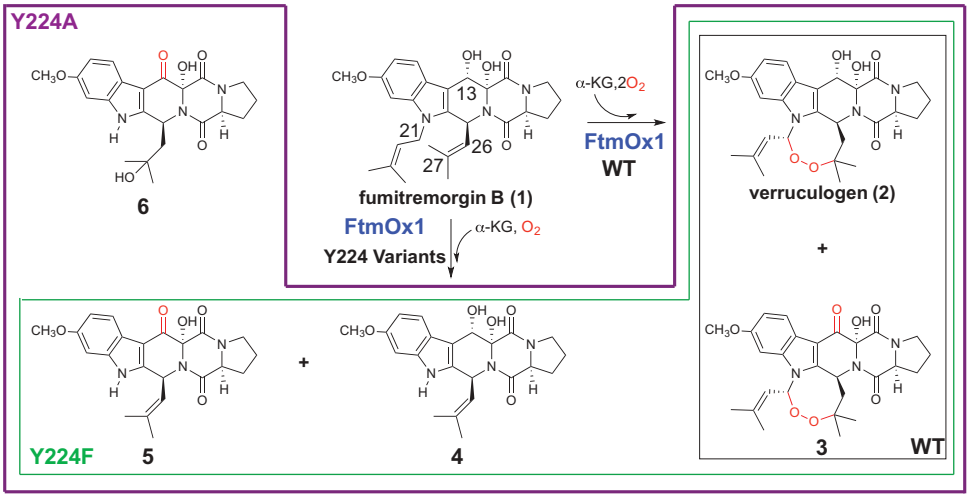

Q18 **Scheme 5:** Observed product distribution in the WT (black box), Y224F (green box), and Y224A (purple box) FtmOx1 reactions.

of artemisinin to fight against malaria is still unknown, it is believed that the active part of the molecule—the unusual endoperoxide bridge—could form free radicals to attack various parasite proteins. Despite the beneficial effects to human health demonstrated by endoperoxide-containing natural products, their biosynthesis, especially endoperoxide formation, is not well understood, which limits the availability of these compounds through chemical synthesis or biosynthesis in engineered organisms. The only well-characterized endoperoxide biosynthetic enzyme is prostaglandin H synthase (COX), which is a heme-containing enzyme (Scheme 4).[117]

FtmOx1 is the first Fe/αKG-dependent enzyme discovered to catalyze the endoperoxide bond formation reaction in the biosynthesis of tremorgenic mycotoxin in *Aspergillus* and *Penicillium* fungus strains. The initial biochemical study on FtmOx1 revealed that this enzyme converts fumitremorgin B (**1**) to verruculogen (**2**) by installing an endoperoxide between two prenyl moieties of fumitremorgin B in an αKG-, O_2- and Fe(II)-dependent fashion (Scheme 4).[62] Most interestingly, O_2 is directly incorporated into verruculogen without O-O bond scission, thus distinguishing FtmOx1 from all currently known Fe/αKG-dependent enzymes.

To gain molecular-level details about this unique transformation, we used a combined biochemical and biophysical approach to unravel the reaction mechanism of FtmOx1.[63] The Fe(II)-loaded heterologously expressed FtmOx1 binds αKG and develops a pink species observed at 520 nm, which originates from the typical MLCT band of the Fe(II)-αKG binary complex in Fe/αKG-dependent enzymes. The dissociation contant of αKG for the Fe(II)

center was determined to be ~ 185 μM, which is similar to those in other Fe/αKG-dependent enzymes, such as TauD.[91] Without the presence of the primary substrate, the FtmOx1-Fe(II)-αKG ternary complex develops a blue chromophore centered at ~ 600 nm (ε_{600} ~ 380 M^{-1} cm^{-1}) after a prolonged incubation with O_2. Tandem mass spectrometry analysis of this species indicated the formation of the dihydroxyphenylalanine (DOPA) from a tyrosine residue (Tyr224). This type of self-hydroxylation reaction has been reported in several Fe/αKG-dependent enzymes. Usually, the kinetics of this type of reaction is slow and its precise mechanism is unknown. It has been suggested in TauD that the self-hydroxylation may go through a tyrosyl radical intermediate.[95] Nonetheless, the observation of DOPA formation strongly suggests that Tyr224 is close to the iron center of FtmOx1.

The FtmOx1-Fe(II)-αKG ternary complex was further subjected to crystallographic studies. A 1.95 Å resolution crystal structure revealed that FtmOx1 exhibits a DSBH fold, which is common for Fe/αKG enzymes (Figure 2). The Fe(II) center is ligated with the conserved 2-His-1-carboxylate facial triad with αKG binding to the Fe(II) in a bi-dentate fashion and an additional water molecule occupying the remaining coordination site. The orientation of αKG adopts the off-line configuration (see Section 2), which is different from many other Fe/αKG enzymes, such as TauD, where an in-line configuration is observed.[71] Indeed, Tyr224 is located in the vicinity of the Fe(II) center and its oxygen atom of the hydroxyl group forms a hydrogen bond interaction with the coordinated water molecule. Although we failed to obtain a crystal structure of the FtmOx1-Fe(II)-αKG-substrate quaternary complex, we did obtain a

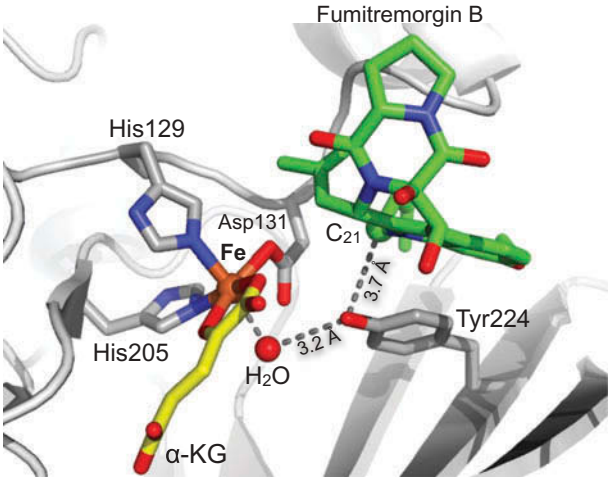

Figure 2: Iron center structure of FtmOx1. The figure was generated by overlaying of the crystal structure of the FtmOx1-Fe(II)-αKG ternary complex (PDB: 4Y5S) with that of the FtmOx1-Fe(II)-substrate complex (PDB: 4ZON).

crystal structure of the FtmOx1-Fe(II)-substrate complex. When compared with the structure of the ternary complex, the overall structure of the iron center was not changed; more importantly, the positioning of Tyr224 was not altered. Rings A and B of the substrate, fumitremorgin B, form π-π stacking with Tyr224. Overlaying the iron centers in these two crystal structures allows us to visualize the relative positioning of the Fe(II) center, Tyr224, and the substrate. The off-line binding mode of αKG creates a situation where the oxo group of the ferryl intermediate (presumably occupying the water position in the FtmOx1-Fe(II)-αKG ternary complex) formed after the initial O_2 activation could be pointing away from the C-H bond of the subtrate that is activated during the catalysis (C21-H). Thus, the positioning of Tyr224 within short distances to both the Fe(II) center (3.2 Å) and the C21 of the substrate (3.7 Å) makes this residue an attractive candidate for playing an important role in FtmOx1 catalysis.

To test this idea, we carried out enzyme assays and performed product analysis. The overall stoichiometry of the reaction shows that the formation of one molecule of verruculogen requires one molecule of fumitremorgin B and αKG and two molecules of O_2. This reaction stoichiometry is distinct from all other characterized Fe/αKG enzymes, where one molecule of O_2 is consumed in a single catalytic cycle. In addition, in our assay conditions, the over-oxidized product **3** rather than verruculogen (**2**) was the dominant product; **3** was not reported in the initial biochemical study. It is likely that, due to the presence of ascorbic acid, a condition used in the initial biochemical study,[62] the over-oxidation was suppressed. In our study, ascorbic acid was omitted; thus, the over-oxidized product may be generated. However, the mechanism of **3** formation is still unknown. Nevertheless, FtmOx1 can carry out endoperoxidation without the addition of any reducing agents in the reaction mixture. The evidence of the direct involvement of Tyr224 in FtmOx1 catalysis came from a site-directed mutagenesis study. Y224F and Y224A variants were shown to convert the activity of FtmOx1 from endoperoxidation to classical hydroxylation/dealkylation to produce **4, 5**, or **6** as the major products.

Based on these observations, we proposed a possible reaction mechanism (Scheme 6). In this mechanism, several radical intermediates are involved: tyrosyl radical, substrate radical, peroxyl radical, and product radical. To provide experimental evidence to support this proposed mechanism, we performed stopped-flow optical absorption spectroscopy (SF-Abs) and freeze quench (FQ) coupled electron paramagnetic resonance spectroscopy (EPR). We observed a transient radical intermediate in the reaction of wild-type FtmOx1 (Figure 3(a)). This intermediate, termed *Int420*, exhibits an optical absorption feature centered at ~ 420 nm, which reached a maximum at ~ 0.2 s and decayed within 3 s. These kinetics matched well with the kinetics of substrate consumption and the product formation determined by chemical quench experiments, indicating that *Int420* is a

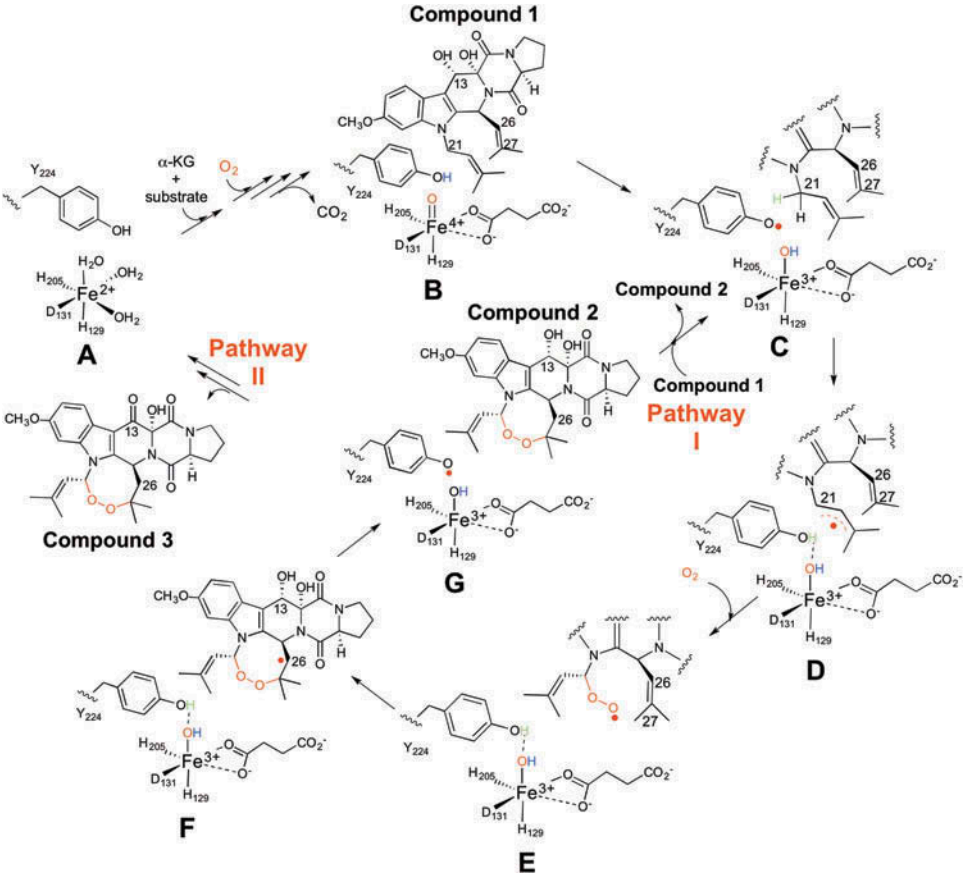

Scheme 6: Proposed reaction mechanism of FtmOx1-catalyzed endoperoxidation.

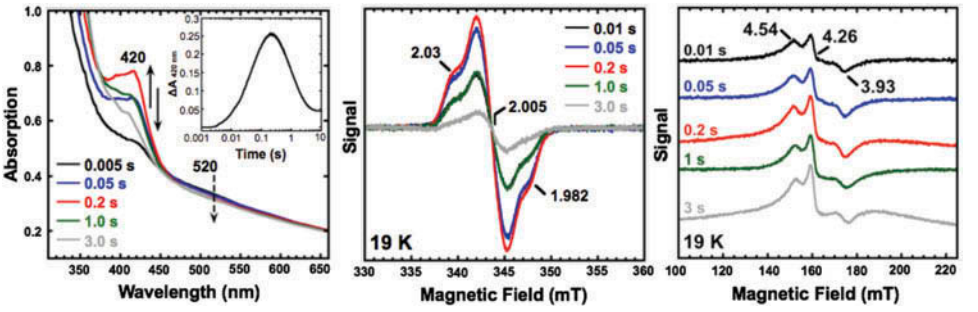

Figure 3: Spectroscopic evidence for a transient radical in the FtmOx1 catalyzed reaction. Left: SF-Abs spectra showing the formation and decay of Int_{420}. The inset shows the 420 nm kinetic trace; middle: the corresponding X-band EPR spectra of Int_{420}; right: the high-spin ferric species formed along with Int_{420}.

kinetically competent intermediate in the FtmOx1 catalysis. More details about this intermediate came from FQ-EPR experiments (Figure 3(b,c)). Two EPR signals were observed at 0.01 s, which maximized at ~ 0.2 s after the rapid mixing of O_2-saturated buffer with the FtmOx1-Fe(II)-αKG-fumitremorginB complex. The first EPR signal with resonances at g = 4.54, 4.26, and 3.93 belongs to a high-spin Fe^{3+} species having axial and rhombic zero-field splitting parameters of $|D| < 0.5\ cm^{-1}$ and E/D ≈ 0.26, respectively. The second EPR signal was in the g = 2 region and most likely belongs to a radical species. The formation and decay of this radical signal closely followed the kinetics of the 420 nm absorption feature observed in SF-Abs experiments, indicating that they are from the same intermediate, *Int420*. Spin quantification of the EPR signals at ~ 0.2 s revealed that the Fe^{3+} and radical species accumulated to ~ 0.35 and ~ 0.25 equivalents, respectively. The width of the radical EPR signal (~ 12 mT edge-to-edge width) was significantly broader than that of magnetically isolated organic or protein radical signals.[118] Such broadening could be due to magnetic dipolar interactions of the radical species with an adjacent spin center, most likely the Fe^{3+} center. Similar radical signal broadening was observed in CarC catalyzed stereo-inversion, where a tyrosyl radical exhibited magnetic broadening in its EPR signal due to magnetic dipolar interactions with the close-by Fe^{3+} center.[53] However, the difference is that Int_{420} in FtmOx1 is less likely to be the tyrosyl radical due to its optical absorption feature, which is distinct from that of a tyrosyl radical species. Instead, the radical signal from Int_{420} could originate from a substrate or product radical.

Although the precise nature of Int_{420} and details of some aspects of the catalytic mechanism of FtmOx1 still await elucidation, our study does provide novel insights into the endoperoxidation reaction catalyzed by an Fe/αKG enzyme. In particular, we have identified Tyr224 as the key protein residue to facilitate the endoperoxidation reaction outcome in FtmOx1. We have also captured and spectroscopically characterized an on-pathway radical intermediate involved in the native reactivity of FtmOx1. Such radical intermediates are rarely observed in Fe/αKG enzymes; the only precedent in the literature is the tyrosyl radical intermediate observed in CarC catalysis.[53] However, in contrast with the CarC case, the radical intermediate observed in FtmOx1 is less likely to be a tyrosyl radical. Furthermore, the decay of this radical species in FtmOx1 leads to the formation of enzyme product. This is in contrast with the tyrosyl radical observed in CarC, which is generated by following the formation of the epimerized product, (3*S*,5*R*)-carbapenam.[53]

One important aspect of the reaction mechanism of FtmOx1 is the exact function of Tyr224. The current hypothesis suggests that it may be oxidized by the ferryl intermediate to form a tyrosyl radical, which is the actual key oxidant to perform the initial C-H activation (Scheme 6). A

recent quantum chemical study supports this hypothesis.[119] However, such a radical species has not been observed. Thermodynamically, this step may be less likely to happen. The reduction potentials of tyrosine in the form of polypeptides and some structured proteins have been determined to be in the range of 0.8 to 1 V at pH 7 in aqueous solution (reference to SHE).[120,121] Although there are no experimental data available on the redox potential of the enzymatic ferryl intermediates in non-heme enzymes, the limited data on synthetic model complexes suggest that the reduction potential of the ferryl species is in the range < 0.5 V (vs. SHE) in acidic aqueous solution.[122,123] However, the precise reduction potentials of both tyrosine and the ferryl intermediate in the protein scaffold of Fe/αKG enzymes are not known, which makes it difficult to rule out the current hypothesis. Another possible function of Tyr224 is to provide a good hydrogen-bonding interaction through the OH group to the Fe(III)-OH species, thus slowing down the OH-rebound step in the FtmOx1 reaction and promoting the O_2 addition to the incipient substrate radical. This hypothesis seems to be supported by the results from the Y224F variant, which is still able to activate the substrate C-H bond but produces mainly the dealkylated product through presumably the OH-rebound pathway. Nevertheless, the current results on FtmOx1 strongly suggest that one of the strategies Fe/αKG enzymes utilize to diversify their reactivity is to strategically place redox active and/or polar residues around the iron center in order to alter the decay pathway of the incipient substrate radical in Fe/αKG enzyme catalysis.

4. THE CONSECUTIVE DESATURATION AND EPOXIDATION REACTIONS CATALYZED BY ASQJ

Viridicatin-type alkaloids consist of a subfamily of naturally abundant quinolone alkaloids. They have been isolated from both terrestrial and marine fungi of the genera *Aspergillus* and *Penicillium*,[124–128] and exhibit pharmaceutically valuable biological activities, including antiviral (including anti-HIV), antibacterial, and antitumor activities.[129–136] Recently, a gene cluster from *Aspergillus nidulans* responsible for the biosynthesis of the viridicatin has been discovered.[137] In this study, an Fe/αKG enzyme, AsqJ, has been identified as the key enzyme to convert 4′-methoxy-cyclopeptin to 4′-methoxy-cyclopenin through sequential desaturation and epoxidation reactions. Subsequently, 4′-methoxy-cyclopenin undergoes an elimination/rearrangement to produce 4′-methoxy-viridicatin (Scheme 7). Thus, AsqJ represents a small sub-family of Fe/αKG enzymes, which exhibit multi-functionality but are not hydroxylases. In addition, although olefin and epoxide are important functional groups found in many bioactive natural products, the reaction

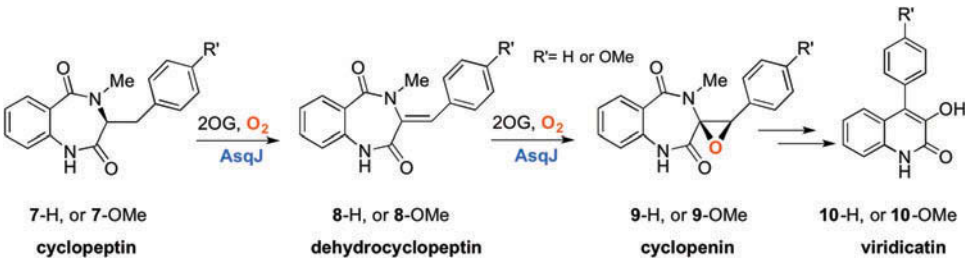

Scheme 7: AsqJ-catalyzed sequential desaturation and epoxidation reactions followed by elimination/rearrangement to yield viridicatin.

mechanisms responsible for the installation of these functional groups catalyzed by Fe/αKG enzymes are not well understood, and the factors that diverge the reactivity from hydroxylation to desaturation and epoxidation have not been carefully elucidated. Using a similar approach described in the study of FtmOx1, and further supplemented with mechanistic probe design, we have obtained several key insights.

4.1. The AsqJ Catalyzed Desaturation

In nature, enzymes that catalyze olefin installation with C-H activation steps typically utilize a metallo- or organic cofactor, such as thiolate heme, di-iron, nonheme-Fe, or flavin, as the reactive center to trigger this chemically challenging transformation. Among them, the desaturation mechanisms in cytochrome P450 enzymes[138,139] and di-iron-containing fatty acyl desaturases[140–142] have been suggested to go through a pathway involving two consecutive hydrogen atom transfers (2-HAT pathway) (Scheme 8a). In Fe/αKG-dependent enzymes, a similar mechanism has been put forward in the studies of clavaminate synthase (CAS)[6,51,143] and flavone synthase I (FNS I).[144] Although it can be envisioned that P450 enzymes and di-iron desaturases carry out 2-HAT by using two potent oxidizing intermediates (Compound I followed by Compound II in P450s, or a (μ-oxo)diiron(IV/IV) species followed by a (μ-oxo)diiron(III/IV) species in di-iron enzymes), it is not obvious how Fe/αKG enzymes can utilize an analogous approach. Specifically, after the initial C-H bond cleavage by a proposed Fe^{IV} = O species, the resulting Fe(III)-OH species may not be potent enough for the second HAT event. Yet, based on the mechanistic studies on lipoxygenase, it has been hypothesized that the resulting Fe(III)-OH species may be suitable for the 2-HAT.[51,145] No direct trapping and characterizations of reactive intermediates to support or disapprove the 2-HAT mechanism have been reported. In addition to the 2-HAT pathway, a carbocation pathway has been proposed in some

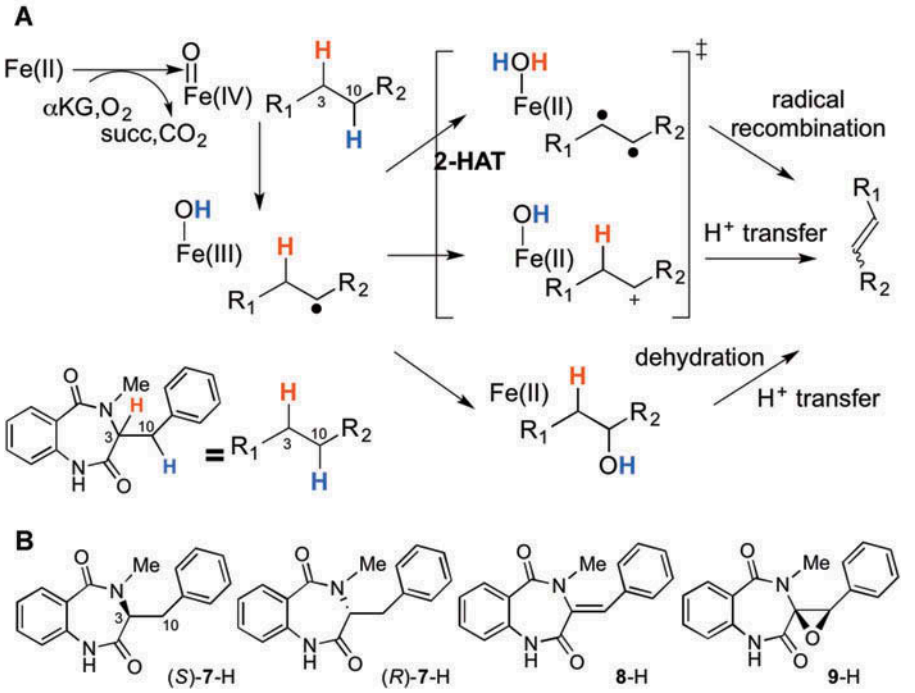

Scheme 8: (A) Possible reaction pathways account for Fe/αKG-catalyzed desaturation reaction. (B) Mechanistic probes and product used to study AsqJ-catalyzed desaturation.

P450 enzymes,[146,147] and a chemical precedent of a hydroxylation/dehydration pathway also needs to be considered (Scheme 8a).

To distinguish among these pathways, we carried out detailed mechanistic studies on AsqJ-catalyzed C = C bond formation by using cyclopeptin [(*S*)-**7**-H], and its C3-stereoisomer, (*R*)-**7**-H (Scheme 8b).[148] Extended incubation of (*S*)-**7**-H or (*R*)-**7**-H with Fe(II) loaded AsqJ in the presence of excess αKG and O_2 led to the complete consumption of both substrates, suggesting that both stereoisomers are the substrate of AsqJ. Interestingly, the formation of cyclopenin (**9**-H), but not the desaturated product, dehydrocyclopeptin, was observed in both cases. To validate the formation of dehydrocyclopeptin as the initial product, chemical quench (CQ) experiments were carried out on both (*S*)-**7**-H or (*R*)-**7**-H. CQ coupled LC-MS analysis clearly demonstrated that, for both stereoisomers, dehydrocyclopeptin (**8**-H) was formed as the major product within a short reaction time (< 2 s), and was further converted to **9**-H in a longer reaction time frame (Figure 4(a)). SF-Abs monitored AsqJ reactions also supported the results obtained from the steady-state enzyme and CQ-LC-MS assays, showing that the decay kinetics of the MLCT feature of the Fe(II)-αKG complex were identical when (*S*)-**7**-H or (*R*)-**7**-H were used. This result suggests that

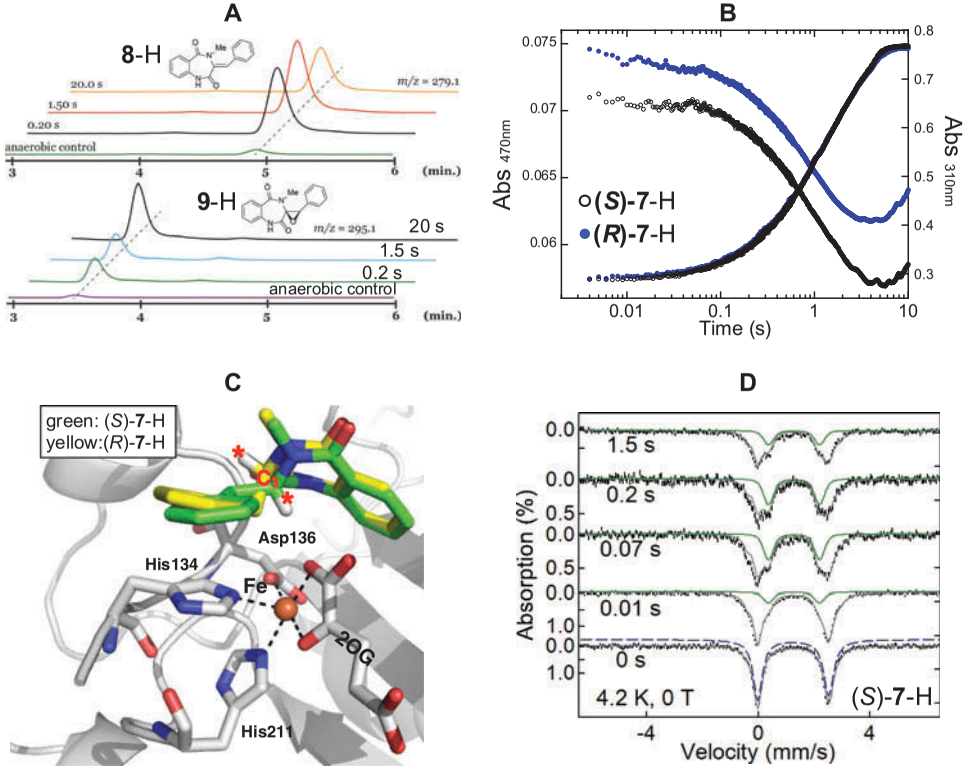

Figure 4: (A) CQ-LC-MS traces showing the formation of **8**-H and the production of **9-H** at the expense of **8-H**. (B) SF-Abs results on the Fe(II)-αKG MLCT band decay (470 nm) and desaturated product formation (310 nm) kinetics, indicating highly similar enzyme kinetics when two C_3-stereoisomers are used. (C) The crystal structures showing the binding configurations of (*S*)-**7**-H (green) and (*R*)-**7**-H (yellow) in the active site of AsqJ. Red asterisk indicates the C3-H position. (D) FQ-Mössbauer spectra showing the formation and decay of the Fe(II)-succinate complex (green) with no observation of the Fe(IV)-oxo species.

the two stereoisomers can trigger αKG consumption with similar efficacy (Figure 4(b)). In addition, a simultaneous increase of absorption at ~ 310 nm was observed, which was attributed to the formation of dehydrocyclopeptin (**8**-H). These results not only confirm the bi-functionality of AsqJ, but also indicate that the C_3-chirality of the substrate does not perturb the enzyme kinetics and product distribution in the AsqJ catalyzed desaturation reaction. To provide structural support of this conclusion, we have recently obtained the crystal structures of (*S*)-**7**-H and (*R*)-**7**-H bound AsqJ with the resolution of 1.96 Å and 2.05 Å, respectively (Figure 4(c)). The overall protein structure as well as the active site geometry are similar to the published Ni-bound AsqJ crystallographic structure (PDB: 5DAW).[149] However, our results represent the first visualization of AsqJ in its native iron-bound form. It also worth noting that the binding configuration of αKG to the iron center in AsqJ is the off-line mode, which is the same as that in FtmOx1. In the (*S*)-**7**-H bound AsqJ, the C_3-H and one of C_{10}-Hs are poised for HAT with iron-carbon distances of 4.5 and 4.8 Å, respectively. In contrast, in the case of (*R*)-**7**-H, only the C_{10}-Hs point toward the iron center; the C_3-H points away from it and poises at the opposite face due to the inversion of C_3-stereochemistry. Thus, the binding configuration of (*R*)-**1**-H implies that C_{10}-H should be the first C-H activation site and the subsequent C-H activation at the C3 position should be abolished. In addition, FQ-Mössbauer experiments showed that no accumulation of the ferryl species was detected when (*S*)-**7**-H or (*R*)-**7**-H was used (Figure 4(d)), which may be attributed to the relatively weak bond strength of the benzylic C-H bond, which results in short lifetime of the ferryl species.

The experimental results summarized in the previous section suggest that the first C-H bond being activated is one of the C_{10}-Hs, and the 2-HAT pathway is unlikely to be utilized by AsqJ. However, to distinguish between the carbocation pathway and the hydroxylation/dehydration pathway, more experimentation is still needed. The tuning of the electronic property of the C_{10} position through the para-substitution effect on the phenyl moiety of the substrate may be an applicable strategy to differentiate these pathways. Since both 4′-methoxy-cyclopeptin and cyclopeptin can be used as substrate by AsqJ and the para position is exposed to the protein surface, as illustrated by the crystal structures, the change of substituent at the para position should not create strong perturbation to the substrate binding. On the other hand, we also need to consider another scenario where the initial C-H activation happens at C_3-H instead of C_{10}-H during regular catalysis. The crystal structure revealed that both C_3-H and one of C_{10}-Hs of (*S*)-**7**-H have similar distances to the iron center (different by 0.3 Å); the C-H bond strengths on both carbons are also similar. Thus, the initial C-H activation may occur from C_3-H when (*S*)-**7**-H is used. Nonetheless, different from FtmOx1, where the endoperoxidation reaction

outcome is enforced by the near-by tyrosine residue, in AsqJ, the catalytic preference of desaturation over hydroxylation seems to rely on the decay pathway of the incipient substrate radical after the initial C-H activation step. More experimentation is needed to reveal more details in this transformation.

4.2. The AsqJ Catalyzed Epoxidation

In thiolate-heme-containing enzymes, such as cytochrome P450s, choloroperoxidases (CPO), and their biomimetic model complexes,[150,151] it is generally accepted that the key intermediate in olefin epoxidation is an Fe(IV)-oxo porphyrin-cation-radical species, Compound I, and the overall reaction proceeds through electrophilic addition. Based on the two-state reactivity of P450 Compound I, computational studies further suggest that the epoxidation could go through a step-wise or a concerted mechanism, depending on which spin-state (doublet or quartet state) of Compound I actually participates in the reaction. However, detailed mechanistic studies on non-heme iron enzyme catalyzed oxygen-addition reactions are much less developed than for its counterpart, thiolate-heme-containing enzymes.

Using AsqJ as a model system, we explored the epoxidation mechanism catalyzed by Fe/αKG enzymes.[152] Dehydrocyclopeptins with two different para-substituents (**8**-OMe and **8**-H) were used as substrates. Both substrates exhibited a similar triggering effect on αKG consumption as determined by the decay kinetics of the Fe-αKG MLCT band (Figure 5(a)). For both cases, FQ-Mössbauer experiments (Figure 5(b)) revealed the accumulation of the ferryl intermediates at early time points (maximal accumulation was observed at 0.03 s). This is the first experimental demonstration that the ferryl intermediate is directly involved in epoxidation in the Fe/αKG enzymes. In addition, the para substitution on the phenyl moiety (-OMe vs. –H) clearly affects the lifetime of the Fe(IV)-oxo species, which was revealed by higher accumulation of such a species (~ 30% accumulation) when **8**-H was used compared to **8**-OMe (~ 20% accumulation, Figure 3(b)). By conducting experiments in an $^{18}O_2/H_2{}^{16}O$ environment, we showed that although the epoxide oxygen originated from O_2, $^{18}O/^{16}O$ isotope scrambling was observed (Figure 5(c)). These results suggest that the ferryl oxygen can exchange with the solvent. More importantly, the amount of O incorporation from solvent depended on the para substitution (~ 20% vs. ~ 80% of ^{16}O incorporation with -OMe vs. –H, Figure 5(c)). This observation is in line with the modulation of the ferryl species life time by the para substitution. In short, these results strongly support the conclusion that the ferryl intermediate is the key reactive species during epoxidation, and a solvent exchangeable oxo-group exists in this reactive

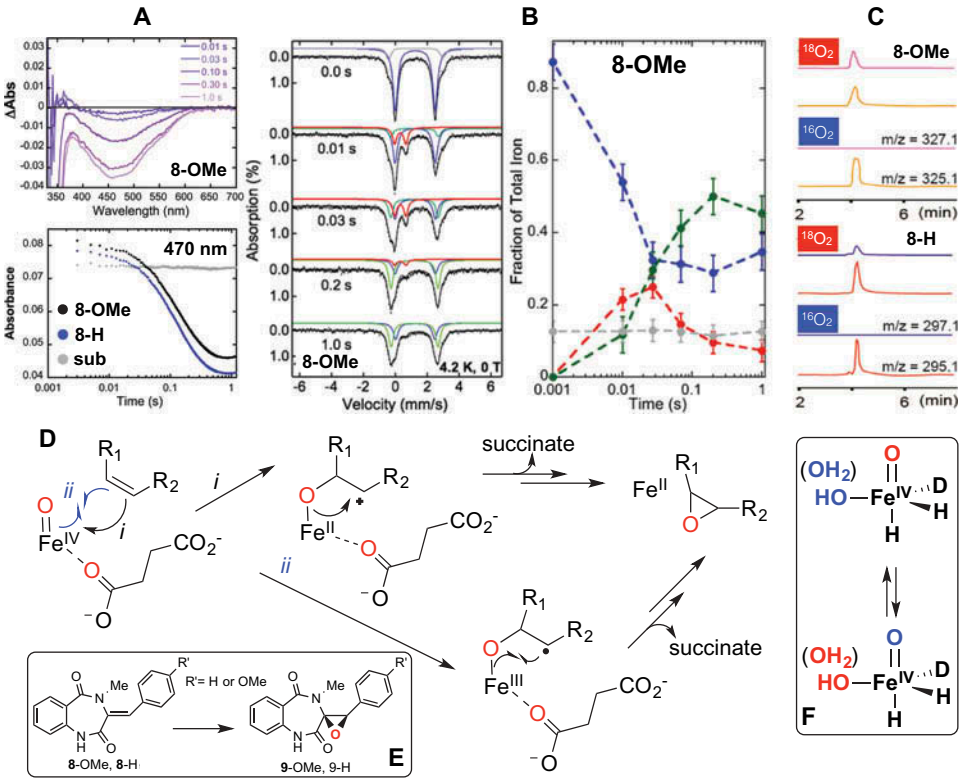

Figure 5: (A) SF-Abs results showing similar Fe(II)-αKG MLCT band decay kinetics by using **2-OMe** and **2-H**, indicating that AsqJ has similar catalytic efficacy when reacting with these two substrates. (B) FQ-Mössbauer results showing the accumulation and decay of Fe^{IV} = O (red traces) using **2**-OMe. (C) LC-MS traces showing the effect of $^{18}O_2$ and $^{16}O_2$ to the product isotope distribution. (D) and (E) Epoxidation mechanisms. (F) Oxo-OH/OH_2 tautomerism at Fe^{IV} = O.

intermediate. Although a solvent exchangeable iron-oxo intermediate has been indicated in heme- and non-heme-containing enzymes[153–158] and biomimetic model complexes,[159–163] our experimental results provided evidence to confirm this oxo-exchange event. This exchange could be modeled by a fast oxo-hydroxo/water tautomerism of the ferryl species (Figure 5(f)). A recent theoretical study on AsqJ using the QM/MM method also supports this conclusion.[83]

It has been well documented in the literature that synthetic non-heme Fe (IV)-oxo species exhibit both HAT and OAT reactivities, depending on the substrates used. Thus, it comes as no surprise that when AsqJ is challenged with the desaturated substrate, dehydrocyclopeptin, where no suitable C-H bond can be cleaved, the alternative epoxidation outcome occurs. Thus, our

study suggests that the intrinsic reactivity of the ferryl intermediate can also dictate the reaction outcomes in Fe/αKG enzyme catalysis.

4.3. AsqJ Catalysis Probed by Mössbauer Spectroscopy

Mössbauer spectroscopy has been used extensively in characterizing the iron center changes during the reactions catalyzed by Fe/αKG enzymes. In fact, the first direct experimental observation of ferryl intermediate was provided by Mössbauer data. So far, a dozen ferryl intermediates have been characterized by Mössbauer spectroscopy. In AsqJ, we have captured the ferryl intermediate in the epoxidation reaction; its Mössbauer parameters closely resemble those of other reported ferryl intermediates.[152] Furthermore, using Mössbauer, we have also observed four different ferrous species in AsqJ catalyzed reactions over the course of our studies.[148,152] A broad quadrupole doublet was observed for the AsqJ-Fe(II)-αKG ternary complex with isomer shift of 1.24 mm/s, quadrupole splittings of 2.24 mm/s, and linewidth of ~ 0.6 mm/s, which reflects a typical high-spin ferrous center. The broad linewidth suggests that the structure of this ternary complex is inhomogeneous, which could result from structural flexibility of the iron center. With the introduction of substrates ((*S*)-**7-H**, (*R*)-**7-H,** 8-OMe, or **8**-H), the AsqJ-Fe(II)-αKG-substrate quaternary complex showed a quadrupole doublet with dramatically sharpened linewidth and altered Mössbauer parameters (Table 1). But the Mössbauer parameters are almost the same for different substrates used. The changes of Mössbauer parameters in going from the ternary complex to the quaternary complex suggest that the substrate binding, although not directly interacting with the iron center, does perturb the iron center structure strongly enough to be detectable by Mössbauer. The

Table 1: Mössbauer simulation parameters of the quaternary complex on various Fe/αKG enzymes

Quaternary Complex	δ (mm/s)[a]	$\lvert\Delta E_Q\rvert$ (mm/s)[a]	Γ (mm/s)[b]	Ref
AsqJ•Fe(II)•αKG•(*S*)-**7-H** (or (*R*)-**7-H**)	1.25	2.54	0.40	148
AsqJ•Fe(II)•αKG•**8**-OMe (or **8**-H)	1.24	2.52	0.36	152
TauD•Fe(II)•αKG•taurine	1.16	2.76	-	66
P4H•Fe(II)•αKG•(Pro-Ala-Pro-Lys)$_3$	1.26	2.39	0.35	101
His99Ala-TauD•Fe(II)•αKG•taurine	1.26	3.44	-	109
	1.21	2.10		
PHD2•Fe(II)•αKG•CODD	1.25	2.16	-	164
	1.28	3.20		
IsnB•Fe(II)•αKG•Trp-NC	1.24	3.09	–0.37	111

[a]Only the magnitudes of quadrupole splittings are listed. [b]Negative linewidth is defined as a convolution of 50% Lorentzian and 50% Gaussian lineshape.

Table 2: Mössbauer simulation parameters of the enzyme-substrate complex on various Fe/αKG enzymes

Enzyme-Product Complex	α (mm/s)[a]	$\lvert\alpha E_Q\rvert$ (mm/s)[a]	Γ (mm/s)[b]	Ref
AsqJ desaturation	1.28	1.83	–0.35	148
AsqJ epoxidation	1.20	2.95	0.33	152
TauD	1.17	2.56	-	67
IsnB	1.15	3.23	–0.30	111

[a]Only the magnitudes of quadrupole splittings are listed. [b]Negative linewidth is defined as a convolution of 50% Lorentzian and 50% Gaussian lineshape.

sharpening of the Mössbauer absorption linewidth for the quaternary complex, when compared with the ternary complex, suggests that, with substrate binding, the structure of the iron center becomes more homogeneous. This observation may be consistent with the previous MCD studies on CAS and TauD, revealing a structural transition from a 6-coordinated iron center to a 5-coordinated one, possibly by the elimination of a water molecule, thus preparing the iron center for rapid addition of O_2.

After the reaction of the AsqJ quaternary complex with O_2, two different enzyme-product complexes were observed by Mössbauer (Table 2), both of which showed a quadrupole doublet typical of a high-spin ferrous species, but with very different parameters from those of the initial quaternary complex. More interestingly, the enzyme-product complex observed in the desaturation reaction can be generated by incubating AsqJ-Fe(II) with succinate and dehydrocyclopeptin (compound **8**) in anaerobic conditions, thus confirming its identity. But the enzyme-product complex observed in the epoxidation reaction is transient, and cannot be reproduced by incubating AsqJ-Fe(II) with succinate and cyclopenin (**9**). The significant differences in the Mössbauer parameters of the two enzyme-product complexes reflect the difference in iron center structures. Based on the current understanding, the desaturation reaction generates an iron-bound water molecule derived from O_2, but in the epoxidation reaction such an iron-bound water molecule does not exist at the conclusion of the reaction. Apparently, more detailed Mössbauer analysis on these ferrous species is needed to further elucidate the structual features of these Fe(II) centers.

5. CLOSING REMARKS

By using a mononuclear iron center ligated with the 2-His-1-carboxylate binding motif, Fe/αKG enzymes demonstrate truly remarkable capabilities in catalyzing diverse reactions. In addition to hydroxylation, other novel oxidative transformations have been discovered over the past decades.

Along with the cytochrome P450 enzyme family, these two enzyme families show great catalytic diversity. In some aspects, Fe/αKG enzymes may be better biocatalysts engineered by nature than cytochrome P450 enzymes, due to the presence of a flexible iron center structure (three iron coordination sites are available for co-substrate and O_2 binding), the utilization of an abundant small molecule metabolite, αKG, and the independence of redox partners in catalysis. It is also intriguing to see that the diverse reactivities of Fe/αKG enzymes are exclusively initiated by the obligatory key intermediate in the catalytic cycle, the ferryl intermediate, with a single spin state accessible in the reaction. This is in strong contrast with cytochrome P450 enzymes, where different reactive species (Compound 0, Compound I, and Compound II) and different spin states of the reactive intermediates (doublet- and quartet-spin states of Compound I) have been postulated to be involved in different catalytic events. Thus, Fe/αKG enzymes present an interesting mechanistic conundrum: how does nature utilize an unapparently simple active center structure via a conserved key reactive intermediate to produce a great complexity in reaction outcomes? The molecular basis for controlling the diverse reaction outcomes becomes the key to unlock this conundrum and to provide molecular-level understanding of Fe/αKG enzyme catalysis. Our studies on FtmOx1 and AsqJ start unraveling some of the strategies utilized by Fe/αKG enzymes, such as the effect of redox/polar residues near the iron center, the electronic properties of the substrate, and the intrinsic reactivity of the ferryl intermediate (HAT vs. OAT). Our studies also illustrate the effectiveness of the combined biochemical and biophysical approach in elucidating Fe/αKG enzyme mechanisms. With the aid of molecular dynamics simulations and quantum chemical calculations, this combined research approach provides a comprehensive understanding of Fe/αKG enzyme catalysis.

FUNDING

This work was supported by grants from Carnegie Mellon University and NSF CHE-1654060 (to YG), and from North Carolina State University; Division of Chemistry; CHE-1654060.

ORCID

Yisong Guo http://orcid.org/0000-0002-4132-3565

REFERENCES

1. Hausinger, R.; Schofield, C., Eds.. *2-Oxoglutarate-Dependent Oxygenases*; The Royal Society of Chemistry, 2015.
2. Martinez, S.; Hausinger, R. P. Catalytic Mechanisms of Fe(II)- and 2-Oxoglutarate-Dependent Oxygenases. *J. Biol. Chem.* **2015**, 290, 20702–20711. DOI: 10.1074/jbc.R115.648691.
3. Ryle, M. J.; Hausinger, R. P. Non-heme iron oxygenases. *Curr. Opin. Chem. Biol.* **2002**, 6, 193–201.
4. Kovaleva, E. G.; Lipscomb, J. D. Versatility of Biological Non-Heme Fe(II) Centers in Oxygen Activation Reactions. *Nat. Chem. Biol.* **2008**, 4, 186–193. DOI: 10.1038/nchembio.71.
5. Costas, M.; Mehn, M. P.; Jensen, M. P.; Que, L., Jr. Oxygen Activation at Mononuclear Nonheme Iron: Enzymes, Intermediates, and Models. *Chem. Rev.* **2004**, 104, 939–986. DOI: 10.1021/cr020628n.
6. Bollinger, J. M., Jr.; Chang, W.; Matthews, M. L.; Martinie, R. J.; Boal, A. K.; Krebs, C. Mechanisms of 2-Oxoglutarate-Dependent Oxygenases: The Hydroxylation Paradigm and Beyond. In *2-Oxoglutarate-Dependent Oxygenases*; Hausinger, R., Schofield, C., Eds.; The Royal Society of Chemistry, 2015; pp 95–122.
7. Trewick, S. C.; Henshaw, T. F.; Hausinger, R. P.; Lindahl, T.; Sedgwick, B. Oxidative Demethylation by Escherichia Coli AlkB Directly Reverts DNA Base Damage. *Nature* **2002**, 419, 174–178. DOI: 10.1038/nature00908.
8. Falnes, P. Ø.; Johansen, R. F.; Seeberg, E. AlkB-Mediated Oxidative Demethylation Reverses DNA Damage in Escherichia Coli. *Nature* **2002**, 419, 178–182. DOI: 10.1038/nature01048.
9. Bratlie, M. S.; Drabløs, F. Bioinformatic Mapping of AlkB Homology Domains in Viruses. *BMC Genomics* **2005**, 6, 1–15. DOI: 10.1186/1471-2164-6-1.
10. Kurowski, M. A.; Bhagwat, A. S.; Papaj, G.; Bujnicki, J. M. Phylogenomic Identification of Five New Human Homologs of the DNA Repair Enzyme AlkB. *BMC Genomics* **2003**, 4, 1–6. DOI: 10.1186/1471-2164-4-48.
11. Muller, T. A.; Hausinger, R. P. AlkB and Its Homologues - DNA Repair and Beyond. In *2-Oxoglutarate-Dependent Oxygenases*; Schofield, C. J., Hausinger, R. P., Eds.; Royal Society of Chemistry, 2015; pp 246–262.
12. Tsukada, Y.; Fang, J.; Erdjument-Bromage, H.; Warren, M. E.; Borchers, C. H.; Tempst, P.; Zhang, Y. Histone Demethylation by a Family of JmjC Domain-Containing Proteins. *Nature* **2006**, 439, 811–816. DOI: 10.1038/nature04340.
13. Whetstine, J. R.; Nottke, A.; Lan, F.; Huarte, M.; Smolikov, S.; Chen, Z.; Spooner, E.; Li, E.; Zhang, G.; Colaiacovo, M.; Shi, Y. Reversal of Histone Lysine Trimethylation by the JMJD2 Family of Histone Demethylases. *Cell* **2006**, 125, 467–481. DOI: 10.1016/j.cell.2006.03.028.
14. Klose, R. J.; Yamane, K.; Bae, Y.; Zhang, D.; Erdjument-Bromage, H.; Tempst, P.; Wong, J.; Zhang, Y. The Transcriptional Repressor JHDM3A Demethylates Trimethyl Histone H3 Lysine 9 and Lysine 36. *Nature* **2006**, 442, 312–316. DOI: 10.1038/nature04853.
15. Cloos, P. A. C.; Christensen, J.; Agger, K.; Maiolica, A.; Rappsilber, J.; Antal, T.; Hansen, K. H.; Helin, K. The Putative Oncogene GASC1 Demethylates Tri- and

Dimethylated Lysine 9 on Histone H3. *Nature* **2006**, 442, 307–311. DOI: 10.1038/nature04837.

16. Chen, Z.; Zang, J.; Whetstine, J.; Hong, X.; Davrazou, F.; Kutateladze, T. G.; Simpson, M.; Mao, Q.; Pan, C. H.; Dai, S.; Hagman, J.; Hansen, K.; Shi, Y.; Zhang, G. Structural Insights into Histone Demethylation by JMJD2 Family Members. *Cell* **2006**, 125, 691–702. DOI: 10.1016/j.cell.2006.04.024.

17. Cheng, X.; Trievel, R. C. JmjC Lysine Demethylases. In *2-Oxoglutarate-Dependent Oxygenases*; Schofield, C. J., Hausinger, R. P., Eds.; Royal Society of Chemistry, 2015; pp 210–245.

18. Jia, G.; Fu, Y.; Zhao, X.; Dai, Q.; Zheng, G.; Yang, Y.; Yi, C.; Lindahl, T.; Pan, T.; Yang, Y.-G.; He, C. N6-Methyladenosine in Nuclear RNA Is a Major Substrate of the Obesity-Associated FTO. *Nat. Chem. Biol.* **2011**, 7, 885–887. DOI: 10.1038/nchembio.687.

19. Zheng, G.; Dahl, J. A.; Niu, Y.; Fedorcsak, P.; Huang, C. M.; Li, C. J.; Vagbo, C. B.; Shi, Y.; Wang, W. L.; Song, S. H.; Lu, Z.; Bosmans, R. P. G.; Dai, Q.; Hao, Y. J.; Yang, X.; Zhao, W. M.; Tong, W. M.; Wang, X. J.; Bogdan, F.; Furu, K.; Fu, Y.; Jia, G.; Zhao, X.; Liu, J.; Krokan, H. E.; Klungland, A.; Yang, Y. G.; He, C. ALKBH5 Is a Mammalian RNA Demethylase that Impacts RNA Metabolism and Mouse Fertility. *Mol. Cell* **2013**, 49, 18–29. DOI: 10.1016/j.molcel.2012.10.015.

20. Zheng, G.; He, C. RNA Demethylation by FTO and ALKBH5. In *2-Oxoglutarate-Dependent Oxygenases*; Schofield, C. J., Hausinger, R. P., Eds.; Royal Society of Chemistry, 2015; pp 263–274.

21. Huang, Y.; Rao, A. Connections between TET Proteins and Aberrant DNA Modification in Cancer. *Trends Genet.* **2014**, 30, 464–474. DOI: 10.1016/j.tig.2014.07.005.

22. Shen, L.; Song, C.-X.; He, C.; Zhang, Y. Mechanism and Function of Oxidative Reversal of DNA and RNA Methylation. *Annu. Rev. Biochem.* **2014**, 83, 585–614. DOI: 10.1146/annurev-biochem-060713-035513.

23. Aravind, L.; Zhang, D.; Iyer, L. M. The TET/JBP Family of Nucleic Acid Base-Modifying 2-Oxoglutarate and Iron-Dependent Dioxygenases. In *2-Oxoglutarate-Dependent Oxygenases*; Schofield, C. J., Hausinger, R. P., Eds.; Royal Society of Chemistry, 2015; pp 289–308.

24. Ivan, M.; Kondo, K.; Yang, H.; Kim, W.; Valiando, J.; Ohh, M.; Salic, A.; Asara, J. M.; Lane, W. S.; Kaelin, W. G. HIFα Targeted for VHL-Mediated Destruction by Poline Hydroxylation: Implications for O_2 Sensing. *Science* **2001**, 292, 464–468. DOI: 10.1126/science.292.5522.1627b.

25. Jaakkola, P.; Mole, D. R.; Tian, Y. M.; Wilson, M. I.; Gielbert, J.; Gaskell, S. J.; Von Kriegsheim, A.; Hebestreit, H. F.; Mukherji, M.; Schofield, C. J.; Maxwell, P. H.; Pugh, C. W.; Ratcliffe, P. J. Targeting of HIF-α to the Von Hippel-Lindau Ubiquitylation Complex by O2-Regulated Prolyl Hydroxylation. *Science* **2001**, 292, 468–472. DOI: 10.1126/science.292.5522.1627b.

26. Schofield, C. J.; Ratcliffe, P. J. Oxygen Sensing by HIF Hydroxylases. *Nat. Rev. Mol. Cell Biol.* **2004**, 5, 343–354. DOI: 10.1038/nrm1366.

27. Wilkins, S. E.; Flashman, E.; Scotti, J. S.; Hopkinson, R. J.; Chowdhury, R.; Schofield, C. J. The Role of 2-Oxoglutarate-Dependent Oxygenases. In *Hypoxia Sensing, in 2-Oxoglutarate-Dependent Oxygenases*; Schofield, C. J., Hausinger, R. P., Eds.; Royal Society of Chemistry, 2015; pp 169–209.

28. Baldwin, J. E.; Abraham, S. E. The Biosynthesis of Penicillins and Cephalosporins. *Nat. Prod. Rep.* **1988**, 5, 129–145. DOI: 10.1039/np9880500129.

29. Kershaw, N. J.; Caines, M. E. C.; Sleeman, M. C.; Schofield, C. J. The Enzymology of Clavam and Carbapenem Biosynthesis. *Chem. Commun.* **2005**, 4251–4263. doi:10.1039/b505964j.

30. Rose, N. R.; McDonough, M. A.; King, O. N. F.; Kawamura, A.; Schofield, C. J. Inhibition of 2-Oxoglutarate Dependent Oxygenases. *Chem. Soc. Rev.* **2011**, 40, 4364–4397. DOI: 10.1039/c0cs00203h.

31. Hutton, J. J.; Tappel, A. L.; Udenfriend, S. Requirements for α-ketoglutarate, Ferrous Ion and Ascorbate by Collagen Proline Hydroxylase. *Biochem. Biophys. Res. Commun.* **1966**, 24, 179–184. DOI: 10.1016/0006-291X(66)90716-9.

32. Rhoads, R. E.; Udenfriend, S. Decarboxylation of Alpha-Ketoglutarate Coupled to Collagen Proline Hydroxylase. *Proc. Natl. Acad. Sci. U. S. A.* **1968**, 60, 1473–1478.

33. Myllylä, R.; Tuderman, L.; Kivirikko, K. I. Mechanism of the Prolyl Hydroxylase Reaction. 2. Kinetic Analysis of the Reaction Sequence. *Eur. J. Biochem.* **1977**, 80, 349–357. DOI: 10.1111/j.1432-1033.1977.tb11889.x.

34. Puistola, U.; Turpeenniemi-Hujanen, T. M.; Myllylä, R.; Kivirikko, K. I. Studies on the Lysyl Hydroxylase Reaction. II. Inhibition Kinetics and the Reaction Mechanism. *Biochim. Biophys. Acta* **1980**, 611, 51–60. DOI: 10.1016/0005-2744(80)90041-8.

35. Kivirikko, K. I.; Pihlajaniemi, T. Collagen Hydroxylases and the Protein Disulfide Isomerase Subunit of Prolyl 4-Hydroxylases. *Adv. Enzymol. Relat. Areas Mol. Biol.* **1998**, 72, 325–398.

36. Hulse, J. D.; Ellis, S. R.; Henderson, M. L. Carnitine Biosynthesis. *J. Biol. Chem.* **1978**, 253, 1654–1659.

37. Vaz, F. M.; Ofman, R.; Westinga, K.; Back, J. W.; Wanders, R. J. A. Molecular and Biochemical Characterization of Rat ε-N-Trimethyllysine Hydroxylase, the First Enzyme of Carnitine Biosynthesis. *J. Biol. Chem.* **2001**, 276, 33512–33517. DOI: 10.1074/jbc.M105929200.

38. Lindstedt, G.; Lindstedt, S.; Olander, B.; Tofft, M. α-Ketoglutarate and Hydroxylation of γ-butyrobetaine. *Biochim. Biophys. Acta* **1968**, 158, 503–505. DOI: 10.1016/0304-4165(68)90317-6.

39. Lindstedt, G.; Lindstedt, S.; Nordin, I. Purification and Properties of γ-Butyrobetaine Hydroxylase from Pseudomonas Sp AK 1. *Biochemistry* **1977**, 16, 2181–2188. DOI: 10.1021/bi00629a022.

40. Hausinger, R. P.;. Biochemical Diversity of 2-Oxoglutarate-Dependent Oxygenases. In *2-Oxoglutarate-Dependent Oxygenases*; Hausinger, R. P., Schofield, C. J., Eds.; The Royal Society of Chemistry, 2015; pp 1–58.

41. Abbott, M. T.; Schandl, E. K.; Lee, R. F.; Parker, T. S.; Midgett, R. J. Cofactor Requirements of Thymine 7-Hydroxylase. *Biochim. Biophys. Acta* **1967**, 132, 525–528. DOI: 10.1016/0005-2744(67)90177-5.

42. Holme, E.; Lindstedt, G.; Lindstedt, S.; Tofft, M. 7-Hydroxylation of Thymine in a Neurospora Strain Coupled to Oxidative Decarboxylation of 2-Ketoglutarate. *Biochim. Biophys. Acta* **1970**, 212, 50–57. DOI: 10.1016/0005-2744(70)90177-4.

43. Holme, E.; Lindstedt, G.; Lindstedt, S.; Tofft, M. 18O Studies of the 2-Ketoglutarate-Dependent Sequential Oxygenation of Thymine to 5-Carboxyuracil. *J. Biol. Chem.* **1971**, 246, 3314–3319.

44. Liu, C. K.; Hsu, C. A.; Abbott, M. T. Catalysis of Three Sequential Dioxygenase Reactions by Thymine 7-Hydroxylase. *Arch. Biochem. Biophys.* **1973**, 159, 180–187. DOI: 10.1016/0003-9861(73)90443-8.

45. Proshlyakov, D. A.; Mccracken, J.; Hausinger, R. P. Spectroscopic Analyses of 2-Oxoglutarate-Dependent Oxygenases : TauD as a Case Study. *J. Biol. Inorg. Chem.* **2017**, 22, 367–379. DOI: 10.1007/s00775-016-1406-3.

46. Bollinger, J. M. J.; Price, J. C.; Hoffart, L. M.; Barr, E. W.; Krebs, C. Mechanism of Taurine: α-ketoglutarate Dioxygenase (Taud) from Escherichia Coli. *Eur. J. Inorg. Chem.* **2005**, 4245–4254. doi:10.1002/ejic.200500476.

47. Aas, P. A.; Otterlei, M.; Falnes, P. Ø.; Vågbø, C. B.; Skorpen, F.; Akbari, M.; Sundheim, O.; Bjørås, M.; Slupphaug, G.; Seeberg, E.; Krokan, H. E. Human and Bacterial Oxidative Demethylases Repair Alkylation Damage in Both RNA and DNA. *Nature* **2003**, 421, 859–863. DOI: 10.1038/nature01363.

48. Salowe, S. P.; Neil Marsh, E.; Townsend, C. A. Purification and Characterization of Clavaminate Synthase from Streptomyces Clavuligerus: An Unusual Oxidative Enzyme in Natural Product Biosynthesis. *Biochemistry* **1990**, 29, 6499–6508. DOI: 10.1021/bi00479a023.

49. Busby, R. W.; Chang, M. D.-T.; Busby, R. C.; Wimp, J.; Townsend, C. A. Expression and Purification of Two Isozymes of Clavaminate Synthase and Initial Characterization of the Iron Binding Site. *J. Biol. Chem.* **1995**, 270, 4262–4269. DOI: 10.1074/jbc.270.9.4262.

50. Pavel, E. G.; Zhou, J.; Busby, R. W.; Gunsior, M.; Townsend, C. A.; Solomon, E. I. Circular Dichroism and Magnetic Circular Dichroism Spectroscopic Studies of the Non-Heme Ferrous Active Site in Clavaminate Synthase and Its Interaction with α-ketoglutarate Cosubstrate. *J. Am. Chem. Soc.* **1998**, 120, 743–753. DOI: 10.1021/ja972408a.

51. Zhou, J.; Kelly, W. L.; Bachmann, B. O.; Gunsior, M.; Townsend, C. A.; Solomon, E. I. Spectroscopic Studies of Substrate Interactions with Clavaminate Synthase 2, a Multifunctional α-KG-dependent Non-Heme Iron Enzyme: Correlation with Mechanisms and Reactivities. *J. Am. Chem. Soc.* **2001**, 123, 7388–7398.

52. Phelan, R. M.; Townsend, C. A. Mechanistic Insights into the Bifunctional Non-Heme Iron Oxygenase Carbapenem Synthase by Active Site Saturation Mutagenesis. *J. Am. Chem. Soc.* **2013**, 135, 7496–7502. DOI: 10.1021/ja311078s.

53. Chang, W.; Guo, Y.; Wang, C.; Butch, S. E.; Rosenzweig, A. C.; Boal, A. K.; Krebs, C.; Bollinger, J. M. J. Mechanism of the C5 Stereoinversion Reaction in the Biosynthesis of Carbapenem Antibiotics. *Science* **2014**, 343, 1140–1144. DOI: 10.1126/science.1248000.

54. Hashimoto, T.; Yamada, Y. Purification and Characterization of Hyoscyamine 6β-Hydroxylase from Root Cultures of Hyoscyamus Niger L. Hydroxylase and Epoxidase Activities in the Enzyme Preparation. *Eur. J. Biochem.* **1987**, 164, 277–285. DOI: 10.1111/j.1432-1033.1987.tb11055.x.

55. Hashimoto, T.; Hayashi, A.; Amano, Y.; Kohno, J.; Iwanari, H.; Usuda, S.; Yamada, Y. Hyoscyamine 6β-Hydroxylase, an Enzyme Involved in Tropane Alkaloid Biosynthesis, Is Localized at the Pericycle of the Root. *J. Biol. Chem.* **1991**, 266, 4648–4653.

56. Hashimoto, T.; Matsuda, J.; Yamada, Y. Two-Step Epoxidation of Hyoscyamine to Scopolamine Is Catalyzed by Bifunctional Hyoscyamine 6β-hydroxylase. *FEBS Lett.* **1993**, 329, 35–39. DOI: 10.1016/0014-5793(93)80187-Y.

57. Ushimaru, R.; Ruszczycky, M. W.; Chang, W.; Yan, F.; Liu, Y.; Liu, H. Substrate Conformation Correlates with the Outcome of Hyoscyamine 6β-Hydroxylase Catalyzed Oxidation Reactions. *J. Am. Chem. Soc.* **2018**, 140, 7433–7436. DOI: 10.1021/jacs.8b03729.

58. Vaillancourt, F. H.; Yin, J.; Walsh, C. T. SyrB2 in Syringomycin E Biosynthesis Is a Nonheme FeII α-ketoglutarate- and O2-Dependent Halogenase. *Proc. Natl. Acad. Sci.* **2005**, 102, 10111–10116. DOI: 10.1073/pnas.0504412102.

59. Matthews, M. L.; Krest, C. M.; Barr, E. W.; Vaillancourt, F. H.; Walsh, C. T.; Green, M. T.; Krebs, C.; Bollinger, J. M. Substrate-Triggered Formation and Remarkable Stability of the C−H Bond-Cleaving Chloroferryl Intermediate in the Aliphatic Halogenase, SyrB2. *Biochemistry* **2009**, 48, 4331–4343. DOI: 10.1021/bi900109z.

60. Ueki, M.; Galonić, D. P.; Vaillancourt, F. H.; Garneau-Tsodikova, S.; Yeh, E.; Vosburg, D. A.; Schroeder, F. C.; Osada, H.; Walsh, C. T. Enzymatic Generation of the Antimetabolite γ,γ-Dichloroaminobutyrate by NRPS and Mononuclear Iron Halogenase Action in a Streptomycete. *Chem. Biol.* **2006**, 13, 1183–1191. DOI: 10.1016/j.chembiol.2006.03.005.

61. Galonić, D. P.; Barr, E. W.; Walsh, C. T.; Bollinger, J. M. J.; Krebs, C. Two Interconverting Fe(IV) Intermediates in Aliphatic Chlorination by the Halogenase CytC3. *Nat. Chem. Biol.* **2007**, 3, 113–116. DOI: 10.1038/nchembio856.

62. Steffan, N.; Grundmann, A.; Afiyatullov, S.; Ruan, H.; Li, S. FtmOx1, a Non-Heme Fe (II) and A-Ketoglutarate-Dependent Dioxygenase, Catalyses the Endoperoxide Formation of Verruculogen in Aspergillus Fumigatus. *Org. Biomol. Chem.* **2009**, 7, 4082–4087. DOI: 10.1039/b816235b.

63. Yan, W.; Song, H.; Song, F.; Guo, Y.; Wu, C.-H.; Sae Her, A.; Pu, Y.; Wang, S.; Naowarojna, N.; Weitz, A.; Hendrich, M. P.; Costello, C. E.; Zhang, L.; Liu, P.; Jessie Zhang, Y. Endoperoxide formation by an α-ketoglutarate-dependent mononuclear non-haem iron enzyme. *Nature* **2015**, 527, 539–543. DOI: 10.1038/nature15724.

64. Lau, W.; Sattely, E. S. Six Enzymes from Mayapple that Complete the Biosynthetic Pathway to the Etoposide Aglycone. *Science* **2015**, 349, 1224–1228. DOI: 10.1126/science.aac7202.

65. Hanauske-Abel, H. M.; Günzler, V. A Stereochemical Concept for the Catalytic Mechanism of Prolylhydroxylase. Applicability to Classification and Design of Inhibitors. *J. Theor. Biol.* **1982**, 94, 421–455. DOI: 10.1016/0022-5193(82)90320-4.

66. Price, J. C.; Barr, E. W.; Tirupati, B.; Bollinger, J. M. J.; Krebs, C. The First Direct Characterization of A High-Valent Iron Intermediate in the Reaction of an α-ketoglutarate-dependent Dioxygenase: A High-Spin Fe(IV) Complex in taurine/α-ketoglutarate Dioxygenase (Taud) from Escherichia Coli. *Biochemistry* **2003**, 42, 7497–7508. DOI: 10.1021/bi030011f.

67. Price, J. C.; Barr, E. W.; Hoffart, L. M.; Krebs, C.; Bollinger, J. M. Kinetic Dissection of the Catalytic Mechanism of Taurine: Alpha-Ketoglutaratedioxygenase (Taud) from Escherichia Coli. *Biochemistry* **2005**, 44, 8138–8147. DOI: 10.1021/bi050227c.

68. Roach, P. L.; Clifton, I. J.; Fulop, V.; Harlos, K.; Barton, G. J.; Hajdu, J.; Andersson, I.; Schofield, C. J.; Baldwin, J. E. Crystal Structure of Isopenicillin N Synthase Is the First from a New Structural Family of Enzymes. *Nature* **1995**, 375.

Q14

69. Valegård, K.; Terwisscha van Scheltinga, A. C.; Lloyd, M. D.; Hara, T.; Ramaswamy, S.; Perrakis, A.; Thompson, A.; Lee, H.-J.; Baldwin, J. E.; Schofield, C. J.; Hajdu, J.; Andersson, I. Structure of a Cephalosporin Synthase. *Nature* **1998**, 394, 805–809. DOI: 10.1038/29522.

70. Zhang, Z.; Ren, J.; Stammers, D. K.; Baldwin, J. E.; Marios, K.; Schofield, C. J. Structural Origins of the Selectivity of the Trifunctional Oxygenase Clavaminic Acid Synthase. *Nat. Struct. Biol.* **2000**, 7, 127–133. DOI: 10.1038/79688.

71. Elkins, J. M.; Ryle, M. J.; Clifton, I. J.; Dunning Hotopp, J. C.; Lloyd, J. S.; Burzlaff, N. I.; Baldwin, J. E.; Hausinger, R. P.; Roach, P. L. X-Ray Crystal Structure of Escherichia Coli taurine/α-ketoglutarate Dioxygenase Complexed to Ferrous Iron and Substrates. *Biochemistry* **2002**, 41, 5185–5192. DOI: 10.1021/bi016014e.

72. Clifton, I. J.; Hsueh, L. C.; Baldwin, J. E.; Harlos, K.; Schofield, C. J. Structure of Proline 3-Hydroxylase: Evolution of the Family of 2-Oxoglutarate Dependent Oxygenases. *Eur. J. Biochem.* **2001**, 268, 6625–6636. DOI: 10.1046/j.0014-2956.2001.02617.x.

73. Hegg, E. L.; Jr, L. Q. The 2-His-1-Carboxylate Facial Triad - an Emerging Structural Motif in Mononuclear Non-Heme Iron(II) Enzymes. *Eur. J. Biochem.* **1997**, 250, 625–629. DOI: 10.1111/ejb.1997.250.issue-3.

74. Martinez, S.; Fellner, M.; Herr, C. Q.; Ritchie, A.; Hu, J.; Hausinger, R. P. Structures and Mechanisms of the Non-Heme Fe(II)- and 2-Oxoglutarate-Dependent Ethylene-Forming Enzyme: Substrate Binding Creates a Twist. *J. Am. Chem. Soc.* **2017**, 139, 11980–11988. DOI: 10.1021/jacs.7b06186.

75. Allpress, C. J.; Kleespies, S. T.; Que, L. J. Synthetic Models of 2-Oxoglutarate-Dependent Oxygenases. In *2-Oxoglutarate-Dependent Oxygenases*; Schofield, C. J., Hausinger, R. P., Eds.; Royal Society of Chemistry, 2015; pp 123–148.

76. Shaik, S.; Hirao, H.; Kumar, D. Reactivity of High-Valent Iron-Oxo Species in Enzymes and Synthetic Reagents: A Tale of Many States. *Acc. Chem. Res.* **2007**, 40, 532–542. DOI: 10.1021/ar600042c.

77. Lai, W.; Li, C.; Chen, H.; Shaik, S. Hydrogen-Abstraction Reactivity Patterns from A to Y: The Valence Bond Way. *Angew. Chem. Int. Ed.* **2012**, 51, 5556–5578. DOI: 10.1002/anie.201108398.

78. Kirchner, B.; Wennmohs, F.; Ye, S.; Neese, F. Theoretical Bioinorganic Chemistry: The Electronic Structure Makes a Difference. *Curr. Opin. Chem. Biol.* **2007**, 11, 134–141. DOI: 10.1016/j.cbpa.2007.02.026.

79. Blomberg, M. R. A.; Borowski, T.; Himo, F.; Liao, R.-Z.; Siegbahn, P. E. M. Quantum Chemical Studies of Mechanisms for Metalloenzymes. *Chem. Rev* **2014**, 114, 3601–3658. DOI: 10.1021/cr400388t.

80. Huang, J.; Li, C.; Wang, B.; Sharon, D. A.; Wu, W.; Shaik, S. Selective Chlorination of Substrates by the Halogenase SyrB2 Is Controlled by the Protein according to a Combined Quantum Mechanics/Molecular Mechanics and Molecular Dynamics Study. *ACS Catal.* **2016**, 2, 2694–2704. DOI: 10.1021/acscatal.5b02825.

81. Pang, X.; Han, K.; Cui, Q. A Simple but Effective Modeling Strategy for Structural Properties of Non-Heme Fe(II) Sites in Proteins: Test of Force Field Models and Application to Proteins in the AlkB Family. *J. Comput. Chem.* **2013**, 34, 1620–1635. DOI: 10.1002/jcc.23420.

82. Su, H.; Sheng, X.; Zhu, W.; Ma, G.; Liu, Y. Mechanistic Insights into the Decoupled Desaturation and Epoxidation Catalyzed by Dioxygenase AsqJ

Involved in the Biosynthesis of Quinolone Alkaloids. *ACS Catal.* **2017**, 7, 5534–5543. DOI: 10.1021/acscatal.7b01606.

83. Song, X.; Lu, J.; Lai, W. Mechanistic Insights into Dioxygen Activation, Oxygen Atom Exchange and Substrate Epoxidation by AsqJ Dioxygenase from Quantum Mechanical/Molecular Mechanical Calculations. *Phys. Chem. Chem. Phys.* **2017**, 19, 20188–20197. DOI: 10.1039/C7CP02687K.
84. Roach, P. L.; Clifton, I. J.; Hensgens, C. M.; Shibata, N.; Schofield, C. J.; Hajdu, J.; Baldwin, J. E. Structure of Isopenicillin N Synthase Complexed with Substrate and the Mechanism of Penicillin Formation. *Nature* **1997**, 387, 827–830. DOI: 10.1038/42990.
85. Burziaff, N. I.; Rutledge, P. J.; Clifton, I. J.; Hensgens, C. M. H.; Pickford, M.; Adlington, R. M.; Roach, P. L.; Baldwin, J. E. The Reaction Cycle of Isopenicillin N Synthase Observed by X-Ray Diffraction. *Nature* **1999**, 401, 721–724. DOI: 10.1038/44400.
86. Blasiak, L. C.; Vaillancourt, F. H.; Walsh, C. T.; Drennan, C. L. Crystal Structure of the Non-Haem Iron Halogenase SyrB2 in Syringomycin Biosynthesis. *Nature* **2006**, 440, 368–371. DOI: 10.1038/nature04544.
87. Wong, C.; Fujimori, D. G.; Walsh, C. T.; Drennan, C. L. Structural Analysis of an Open Active Site Conformation of Nonheme Iron Halogenase CytC3. *J. Am. Chem. Soc.* **2009**, 131, 4872–4879. DOI: 10.1021/ja8097355.
88. Mitchell, A. J.; Zhu, Q.; Maggiolo, A. O.; Ananth, N. R.; Hillwig, M. L.; Liu, X.; Boal, A. K. Structural Basis for Halogenation by Iron- and 2-Oxo-Glutarate-Dependent Enzyme WelO5. *Nat. Chem. Biol.* **2016**, 12, 636–640. DOI: 10.1038/nchembio.2044.
89. Solomon, E. I.; Brunold, T. C.; Davis, M. I.; Kemsley, J. N.; Lee, S. K.; Lehnert, N.; Neese, F.; Skulan, A. J.; Yang, Y. S.; Zhou, J. Geometric and Electronic Structure/Function Correlations in Non-Heme Iron Enzymes. *Chem. Rev* **2000**, 100, 235–350. DOI: 10.1021/cr9900275.
90. Neidig, M. L.; Brown, C. D.; Light, K. M.; Fujimori, D. G.; Nolan, E. M.; Price, J. C.; Barr, E. W.; Bollinger, J. M.; Krebs, C.; Walsh, C. T.; Solomon, E. I. CD and MCD of CytC3 and Taurine Dioxygenase: Role of the Facial Triad in α-KG-dependent Oxygenases. *J. Am. Chem. Soc.* **2007**, 129, 14224–14231. DOI: 10.1021/ja074557r.
91. Ryle, M. J.; Padmakumar, R.; Hausinger, R. P. Stopped-Flow Kinetic Analysis of Escherichia Coli Taurine/Alpha-Ketoglutarate Dioxygenase: Interactions with Alpha-Ketoglutarate, Taurine, and Oxygen. *Biochemistry* **1999**, 38, 15278–15286. DOI: 10.1021/bi9912746.
92. Aik, W. S.; Chowdhury, R.; Clifton, I. J.; Hopkinson, R. J.; Leissing, T.; McDonough, M. A.; Nowak, R.; Schofield, C. J.; Walport, L. J. Introduction to Structural Studies on 2-Oxoglutarate-Dependent Oxygenases and Related Enzymes. In *2-Oxoglutarate-Dependent Oxygenases*; Hausinger, R. P., Schofield, C. J., Eds.; The Royal Society of Chemistry, 2015; pp 59–94.
93. Martinez, S.; Hausinger, R. P. Biochemical and Spectroscopic Characterization of the Non-Heme Fe(II)- and 2-Oxoglutarate-Dependent Ethylene-Forming Enzyme from Pseudomonas Syringae Pv. Phaseolicola PK2. *Biochemistry* **2016**, 55, 5989–5999. DOI: 10.1021/acs.biochem.5b01207.
94. Martinez, S.; Hausinger, R. P. Correction to Biochemical and Spectroscopic Characterization of the Non-Heme Fe(II)- and 2-Oxoglutarate-Dependent

Q16

Ethylene-Forming Enzyme from Pseudomonas Syringae Pv. Phaseolicola PK2. *Biochemistry* **2017**, 56, 3158. DOI: 10.1021/acs.biochem.7b00502.

95. Ryle, M. J.; Liu, A.; Muthukumaran, R. B.; Ho, R. Y. N.; Koehntop, K. D.; McCracken, J.; Que, L.; Hausinger, R. P. O2- and α-ketoglutarate-dependent Tyrosyl Radical Formation in TauD, an α-keto Acid-Dependent Non-Heme Iron Dioxygenase. *Biochemistry* **2003**, 42, 1854–1862. DOI: 10.1021/bi026832m.

96. Mitchell, A. J.; Dunham, N. P.; Martinie, R. J.; Bergman, J. A.; Pollock, C. J.; Hu, K.; Allen, B. D.; Chang, W. C.; Silakov, A.; Bollinger, J. M.; Krebs, C.; Boal, A. K. Visualizing the Reaction Cycle in an Iron(II)- and 2-(Oxo)-Glutarate-Dependent Hydroxylase. *J. Am. Chem. Soc.* **2017**, 139, 13830–13836. DOI: 10.1021/jacs.7b07374.

97. Ye, S.; Riplinger, C.; Hansen, A.; Krebs, C.; Bollinger, J. M.; Neese, F.; Ii, F. Electronic Structure Analysis of the Oxygen-Activation Mechanism by Fe II- and α-ketoglutarate (αKG)-dependent Dioxygenases. *Chem. - A Eur. J.* **2012**, 18, 6555–6567. DOI: 10.1002/chem.201102829.

98. Wójcik, A.; Radoń, M.; Borowski, T. Mechanism of O2 Activation by α-Ketoglutarate Dependent Oxygenases Revisited. A Quantum Chemical Study. *J. Phys. Chem. A* **2016**, 120, 1261–1274. DOI: 10.1021/acs.jpca.5b12311.

99. Borowski, T.; Bassan, A.; Siegbahn, P. E. M. Mechanism of Dioxygen Activation in 2-Oxoglutarate-Dependent Enzymes: A Hybrid DFT Study. *Chem. - A Eur. J.* **2004**, 10, 1031–1041. DOI: 10.1002/chem.200305306.

100. Panay, A. J.; Lee, M.; Krebs, C.; Bollinger, J. M.; Fitzpatrick, P. F. Evidence for a High-Spin Fe(IV) Species in the Catalytic Cycle of a Bacterial Phenylalanine Hydroxylase. *Biochemistry* **2011**, 50, 1928–1933. DOI: 10.1021/bi1019868.

101. Hoffart, L. M.; Barr, E. W.; Guyer, R. B.; Bollinger, J. M. J.; Krebs, C. Direct Spectroscopic Detection of a C-H-cleaving High-Spin Fe(IV) Complex in a Prolyl-4-Hydroxylase. *Proc. Natl. Acad. Sci. U. S. A.* **2006**, 103, 14738–14743. DOI: 10.1073/pnas.0604005103.

102. Sinnecker, S.; Slep, L. D.; Bill, E.; Neese, F. Performance of Nonrelativistic and Quasi-Relativistic Hybrid DFT for the Prediction of Electric and Magnetic Hyperfine Parameters in 57fe Mössbauer Spectra. *Inorg. Chem.* **2005**, 44, 2245–2254. DOI: 10.1021/ic048609e.

103. Eser, B. E.; Barr, E. W.; Frantom, P. A.; Saleh, L.; Bollinger, J. M., Jr; Krebs, C.; Fitzpatrick, P. F. Direct Spectroscopic Evidence for a High-Spin Fe (IV) Intermediate in Tyrosine Hydroxylase. *J. Am. Chem. Soc* **2007**, 129, 11334–11335. DOI: 10.1021/ja074446s.

104. Fujimori, D. G.; Barr, E. W.; Matthews, M. L.; Koch, G. M.; Yonce, J. R.; Walsh, C. T.; Bollinger, J. M. J.; Krebs, C.; Riggs-Gelasco, P. J.; Galonic, D.; Barr, E. W.; Matthews, M. L.; Koch, G. M.; Yonce, J. R.; Walsh, C. T.; Bollinger, J. M. J.; Krebs, C.; Riggs-Gelasco, P. J. Spectroscopic Evidence for a High-Spin Br-Fe(IV) -Oxo Intermediate in the α-Ketoglutarate-Dependent Halogenase CytC3 from Streptomyces. *J. Am. Chem. Soc.* **2007**, 129, 13408–13409. DOI: 10.1021/ja076454e.

105. Riggs-Gelasco, P. J.; Price, J. C.; Guyer, R. B.; Brehm, J. H.; Barr, E. W.; Martin, B. J.; Krebs, C. EXAFS Spectroscopic Evidence for an FeO Unit in the Fe(IV) Intermediate Observed during Oxygen Activation by Taurine:α-Ketoglutarate Dioxygenase. *J. Am. Chem. Soc.* **2004**, 126, 8108–8109. DOI: 10.1021/ja047044i.

106. Proshlyakov, D. A.; Henshaw, T. F.; Monterosso, G. R.; Ryle, M. J.; Hausinger, R. P. Direct Detection of Oxygen Intermediates in the Non-Heme Fe Enzyme

Taurine/α-Ketoglutarate Dioxygenase. *J. Am. Chem. Soc.* **2004**, 126, 1022–1023. DOI: 10.1021/ja047044i.

107. Grzyska, P. K.; Appelman, E. H.; Hausinger, R. P.; Proshlyakov, D. A. Insight into the Mechanism of an Iron Dioxygenase by Resolution of Steps following the FeIV=HO Species. *Proc. Natl. Acad. Sci. U. S. A.* **2010**, 107, 3982–3987. DOI: 10.1073/pnas.0910097107.

108. Wong, S. D.; Srnec, M.; Matthews, M. L.; Liu, L. V.; Kwak, Y.; Park, K.; Bell, C. B.; Alp, E. E.; Zhao, J.; Yoda, Y.; Kitao, S.; Seto, M.; Krebs, C.; Bollinger, J. M.; Solomon, E. I. Elucidation of the Fe(IV)=O Intermediate in the Catalytic Cycle of the Halogenase SyrB2. *Nature* **2013**, 499, 320–323. DOI: 10.1038/nature12304.

109. Sinnecker, S.; Svensen, N.; Barr, E. W.; Ye, S.; Bollinger, J. M.; Neese, F.; Krebs, C. Spectroscopic and Computational Evaluation of the Structure of the High-Spin Fe(IV)-oxo Intermediates in Taurine: α-ketoglutarate Dioxygenase from Escherichia Coli and Its His99Ala Ligand Variant. *J. Am. Chem. Soc.* **2007**, 129, 6168–6179. DOI: 10.1021/ja067899q.

110. Price, J. C.; Barr, E. W.; Glass, T. E.; Krebs, C.; Bollinger, J. M. J. Evidence for Hydrogen Abstraction from C1 of Taurine by the High-Spin Fe(IV) Intermediate Detected during Oxygen Activation by Taurine:α-Ketoglutarate Dioxygenase (Taud). *J. Am. Chem. Soc.* **2003**, 125, 13008–13009. DOI: 10.1021/ja0263137.

111. Huang, J.-L.; Tang, Y.; Yu, C.-P.; Sanyal, D.; Jia, X.; Liu, X.; Guo, Y.; Chang, W. Mechanistic Investigation of Oxidative Decarboxylation Catalyzed by Two Iron (II)- and 2-Oxoglutarate-Dependent Enzymes. *Biochemistry* **2018**, 57, 1838–1841. DOI: 10.1021/acs.biochem.8b00115.

112. Groves, J. T.; Van der Puy, M. Stereospecific Aliphatic Hydroxylation by Iron-Hydrogen Peroxide. Evidence for a Stepwise Process. *J. Am. Chem. Soc.* **1976**, 98, 5290–5297. DOI: 10.1021/ja00433a039.

113. Casteel, D. A.;. Peroxy Natural Products. *Nat. Prod. Rep.* **1999**, 16, 55–73. DOI: 10.1039/a705725c.

114. Dembitsky, V. M.;. Bioactive Peroxides as Potential Therapeutic Agents. *Eur. J. Med. Chem.* **2008**, 43, 223–251. DOI: 10.1016/j.ejmech.2007.04.019.

115. Paddon, C. J.; Keasling, J. D. Semi-Synthetic Artemisinin: A Model for the Use of Synthetic Biology in Pharmaceutical Development. *Nat Rev Micro 12.* **2014**, 355–367. doi:10.1038/nrmicro3240.

116. Chaturvedi, D.; Goswami, A.; Saikia, P. P.; Barua, N. C.; Rao, P. G. Artemisinin and Its Derivatives: A Novel Class of Anti-Malarial and Anti-Cancer Agents. *Chem. Soc. Rev.* **2010**, 39, 435–454. DOI: 10.1039/B816679J.

117. Marnett, L. J.;. Cyclooxygenase Mechanisms. *Curr. Opin. Chem. Biol.* **2000**, 4, 545–552. DOI: 10.1016/S1367-5931(00)00130-7.

118. Stubbe, J.; van der Donk, W. A. Protein Radicals in Enzyme Catalysis. *Chem. Rev.* **1998**, 98, 705–762. DOI: 10.1021/cr9400875.

119. Wang, X.; Su, H.; Liu, Y. Insights into the Unprecedented Epoxidation Mechanism of Fumitremorgin B Endoperoxidase (Ftmox1) from Aspergillus Fumigatus by QM/MM Calculations. *Phys. Chem. Chem. Phys.* **2017**, 19, 7668–7677. DOI: 10.1039/C7CP00313G.

120. Ravichandran, K. R.; Liang, L.; Stubbe, J.; Tommos, C. Formal Reduction Potential of 3,5-Difluorotyrosine in a Structured Protein: Insight into Multistep Radical Transfer. *Biochemistry* **2013**, 52, 8907–8915. DOI: 10.1021/bi401494f.

121. DeFelippis, M. R.; Murthy, C. P. B.; Weinraub, D.; Faraggi, M.; Klapper, M. H. Electrochemical Properties of Tyrosine Phenoxy and Tryptophan Indolyl Radicals in Peptides and Amino Acid Analogs. *J. Phys. Chem.* **1991**, 95, 3416–3419. DOI: 10.1021/j100161a081.

122. Wang, D.; Zhang, M.; Bühlmann, P.; Que, L. Redox Potential and C-H Bond Cleaving Properties of a Nonheme Fe(IV)=O Complex in Aqueous Solution. *J. Am. Chem. Soc.* **2010**, 132, 7638–7644. DOI: 10.1021/ja909923w.

123. Nam, W.; Lee, Y. M.; Fukuzumi, S. Tuning Reactivity and Mechanism in Oxidation Reactions by Mononuclear Nonheme iron(IV)-oxo Complexes. *Acc. Chem. Res.* **2014**, 47, 1146–1154. DOI: 10.1021/ar400258p.

124. Cunningham, K. G.; Freeman, G. G. The Isolation and Some Chemical Properties of Viridicatin, a Metabolic Product of Penicillium Viridicatum Westling. *Biochem. J.* **1953**, 53, 328–332. DOI: 10.1042/bj0530328.

125. Raistrick, H.; Robinson, R.; Todd, A. R. Studies in the Biochemistry of Micro-Organisms. *Biochem. J.* **1963**, 89, 196–202.

126. Simonetti, S. O.; Larghi, E. L.; Kaufman, T. S. The 3,4-Dioxygenated 5-Hydroxy-4-Aryl-Quinolin-2(1h)-One Alkaloids. Results of 20 Years of Research, Uncovering a New Family of Natural Products. *Nat. Prod. Rep.* **2016**, 33, 1425–1446. DOI: 10.1039/C6NP00064A.

127. Ahmed, A.; Daneshtalab, M. Nonclassical Biological Activities of Quinolone Derivatives. *J. Pharm. Pharm. Sci.* **2011**, 15, 52–72. DOI: 10.18433/J3302N.

128. Michael, J. P.;. Quinoline, Quinazoline and Acridone Alkaloids. *Nat. Prod. Rep.* **2007**, 24, 223. DOI: 10.1039/b509528j.

129. Heguy, A.; Cai, P.; Meyn, P.; Houck, D.; Russo, S.; Michitsch, R.; Pearce, C.; Katz, B.; Bringmann, G.; Feineis, D.; Taylor, D.; Tyms, A. Isolation and Characterization of the Fungal Metabolite 3-O-Methylviridicatin as an Inhibitor of Tumour Necrosis Factor -Induced Human Immunodeficiency Virus Replication. *Antivir. Chem. Chemother.* **1998**, 9, 149–155. DOI: 10.1177/095632029800900206.

130. Capell, B. C.; Olive, M.; Michael, R.; Cao, K.; Faddah, D. A.; Tavarez, U. L.; Karen, N.; Qu, X.; San, H.; Ganesh, S. K.; Avallone, H.; Kolodgie, F. D.; Virmani, R.; Nabel, E. G.; Collins, F. S.; Capell, B. C.; Olive, M.; Erdos, M. R.; Cao, K.; Faddah, D. A.; Tavarez, U. L.; Conneely, K. N.; Qu, X.; San, H.; Ganesh, S. K.; Chen, X.; Avallone, H.; Kolodgie, F. D.; Virmani, R.; Nabel, E. G.; Collins, F. S. A Farnesyltransferase Inhibitor Prevents Both the Onset and Late Progression of Cardiovascular Disease in A Progeria Mouse Model. *Proc. Natl. Acad. Sci.* **2008**, 105, 15902–15907. DOI: 10.1073/pnas.0807840105.

131. Angibaud, P. R.; Venet, M. G.; Filliers, W.; Broeckx, R.; Ligny, Y. A.; Muller, P.; Poncelet, V. S.; End, D. W. Synthesis Routes Towards the Farnesyl Protein Transferase Inhibitor ZARNESTRA. *European J. Org. Chem.* **2004**, 2, 479–486. DOI: 10.1002/ejoc.200300538.

132. Andresen, B. M.; Couturier, M.; Cronin, B.; D'Occhio, M.; Ewing, M. D.; Guinn, M.; Hawkins, J. M.; Jasys, V. J.; LaGreca, S. D.; Lyssikatos, J. P.; Moraski, G.; Ng, K.; Raggon, J. W.; Stewart, A. M.; Tickner, D. L.; Tucker, J. L.; Urban, F. J.; Vazquez, E.; Wei, L. Streamlined Processes for the Synthesis of a Farnesyl Transferase Inhibitor Drug Candidate. *Org. Process Res. Dev.* **2004**, 8, 643–650. DOI: 10.1021/op049935g.

133. Wall, M. J.; Chen, J.; Meegalla, S.; Ballentine, S. K.; Wilson, K. J.; DesJarlais, R. L.; Schubert, C.; Chaikin, M. A.; Crysler, C.; Petrounia, I. P.; Donatelli, R. R.;

Yurkow, E. J.; Boczon, L.; Mazzulla, M.; Player, M. R.; Patch, R. J.; Manthey, C. L.; Molloy, C.; Tomczuk, B.; Illig, C. R. Synthesis and Evaluation of Novel 3,4,6-Substituted 2-Quinolones as FMS Kinase Inhibitors. *Bioorganic Med. Chem. Lett.* **2008**, 18, 2097–2102. DOI: 10.1016/j.bmcl.2008.01.088.

134. Hewawasam, P.; Fan, W.; Ding, M.; Flint, K.; Cook, D.; Goggins, G. D.; Myers, R. A.; Gribkoff, V. K.; Boissard, C. G.; Dworetzky, S. I.; Starrett, J. E.; Lodge, N. J. 4-Aryl-3-(Hydroxyalkyl)Quinolin-2-Ones: Novel maxi-K Channel Opening Relaxants of Corporal Smooth Muscle Targeted for Erectile Dysfunction. *J. Med. Chem.* **2003**, 46, 2819–2822. DOI: 10.1021/jm030005h.

135. Cappelli, A.; Mohr, G. L. P.; Gallelli, A.; Rizzo, M.; Anzini, M.; Vomero, S.; Mennuni, L.; Ferrari, F.; Makovec, F.; Menziani, M. C.; De Benedetti, P. G.; Giorgi, G. Design, Synthesis, Structural Studies, Biological Evaluation, and Computational Simulations of Novel Potent AT1 Angiotensin II Receptor Antagonists Based on the 4-Phenylquinoline Structure. *J. Med. Chem.* **2004**, 47, 2574–2586. DOI: 10.1021/jm031100t.

136. Ribeiro, N.; Tabaka, H.; Peluso, J.; Fetzer, L.; Nebigil, C.; Dumont, S.; Muller, C. D.; Désaubry, L. Synthesis of 3-O-Methylviridicatin Analogues with Improved anti-TNF-α Properties. *Bioorganic Med. Chem. Lett.* **2007**, 17, 5523–5524. DOI: 10.1016/j.bmcl.2007.08.036.

137. Ishikawa, N.; Tanaka, H.; Koyama, F.; Noguchi, H.; Wang, C. C. C.; Hotta, K.; Watanabe, K. Non-Heme Dioxygenase Catalyzes Atypical Oxidations of 6,7-Bicyclic Systems to Form the 6,6-Quinolone Core of Viridicatin-Type Fungal Alkaloids. *Angew. Chem. Int. Ed.* **2014**, 53, 12880–12884. DOI: 10.1002/anie.201407920.

138. Meunier, B.; De Visser, S. P.; Shaik, S. Mechanism of Oxidation Reactions Catalyzed by Cytochrome P450 Enzymes. *Chem. Rev.* **2004**, 104, 3947–3980. DOI: 10.1021/cr020443g.

139. Kumar, D.; De Visser, S. P.; Shaik, S. Oxygen Economy of Cytochrome P450: What Is the Origin of the Mixed Functionality as a Dehydrogenase-Oxidase Enzyme Compared with Its Normal Function? *J. Am. Chem. Soc.* **2004**, 126, 5072–5073. DOI: 10.1021/ja047044i.

140. Fox, B. G.; Lyle, K. S.; Rogge, C. E. Reactions of the Diiron Enzyme Stearoyl-Acyl Carrier Protein Desaturase. *Acc. Chem. Res.* **2004**, 37, 421–429. DOI: 10.1021/ar0200899.

141. Abad, J. L.; Camps, F.; Fabriàs, G. Substrate-Dependent Stereochemical Course of the (Z)-13-Desaturation Catalyzed by the Processionary Moth Multifunctional Desaturase. *J. Am. Chem. Soc.* **2007**, 129, 15007–15012. DOI: 10.1021/ja0751936.

142. Abad, J. L.; Camps, F.; Fabriàs, G. Is Hydrogen Tunneling Involved in AcylCoA Desaturase Reactions? the Case of a Δ9 Desaturase that Transforms (E)-11-Tetradecenoic Acid into (Z,E)-9,11-Tetradecadienoic Acid. *Angew. Chem. Int. Ed.* **2000**, 39, 3279–3281. DOI: 10.1002/(ISSN)1521-3773.

143. Solomon, E. I.; Decker, A.; Lehnert, N. Non-Heme Iron Enzymes: Contrasts to Heme Catalysis. *Proc. Natl. Acad. Sci. U. S. A.* **2003**, 100, 3589–3594. DOI: 10.1073/pnas.0336792100.

144. Britsch, L.;. Purification and Characterization of Flavone Synthase I, a 2-Oxoglutarate-Dependent Desaturase. *Arch. Biochem. Biophys.* **1990**, 282, 152–160.

145. Pau, M. Y. M.; Lipscomb, J. D.; Solomon, E. I. Substrate Activation for O2 Reactions by Oxidized Metal Centers in Biology. *Proc. Natl. Acad. Sci. U. S. A.* **2007**, 104, 18355–18362. DOI: 10.1073/pnas.0704191104.

146. Rettie, A. E.; Sheffels, P. R.; Korzekwa, K. R.; Gonzalez, F. J.; Philpot, R. M.; Baillie, T. A. CYP4 Isozyme Specificity and the Relationship between Omega-Hydroxylation and Terminal Desaturation of Valproic Acid. *Biochemistry* **1995**, 34, 7889–7895. DOI: 10.1021/bi00024a013.

147. Newcomb, M.; Shen, R.; Choi, S. Y.; Toy, P. H.; Hollenberg, P. F.; Vaz, A. D. N.; Coon, M. J. Cytochrome P450-Catalyzed Hydroxylation of Mechanistic Probes that Distinguish between Radicals and Cations. Evidence for Cationic but Not for Radical Intermediates. *J. Am. Chem. Soc.* **2000**, 122, 2677–2686.

148. Liao, H.-J.; Li, J.; Huang, J.-L.; Davidson, M.; Kurnikov, I.; Lin, T.-S.; Lee, J. L.; Kurnikova, M.; Guo, Y.; Chan, N.-L.; Chang, W. Insights into the Desaturation of Cyclopeptin and Its C3 Epimer Catalyzed by a non-Heme Iron Enzyme: Structural Characterization and Mechanism Elucidation. *Angew. Chem. Int. Ed.* **2018**, 57, 1831–1835. DOI: 10.1002/anie.201710567.

149. Bräuer, A.; Beck, P.; Hintermann, L.; Groll, M.; Multistep, P.; Antibiotic, Q. Structure of the Dioxygenase AsqJ: Mechanistic Insights into a One-Pot Multistep Quinolone Antibiotic Biosynthesis. *Angew. Chem. Int. Ed.* **2016**, 55, 422–426. DOI: 10.1002/anie.201507835.

150. Ortiz De Montellano, P. R.;. Substrate Oxidation by Cytochrome P450 Enzymes. In *Cytochrome P450 Structures, Mechanism, and Biochemistry*, 4th ed.; Ortiz De Montellano, P. R., Ed.; Springer: New York, 2015; pp 111–176.

151. Poulos, T. L.;. Heme Enzyme Structure and Function. *Chem. Rev.* **2014**, 114, 3919–3962. DOI: 10.1021/cr400415k.

152. Chang, W.; Li, J.; Lee, J. L.; Cronican, A. A.; Guo, Y. Mechanistic Investigation of a Non-Heme Iron Enzyme Catalyzed Epoxidation in (-)-4′-Methoxycyclopenin Biosynthesis. *J. Am. Chem. Soc.* **2016**, 138, 10390–10393. DOI: 10.1021/jacs.6b05400.

153. Lindblad, B.; Lindstedt, G.; Lindstedt, S. The Mechanism of Enzymatic Formation of Homogentisate from p-Hydroxyphenylpyruvate. *J. Am. Chem. Soc.* **1970**, 92, 7446–7449. DOI: 10.1021/ja00728a032.

154. Liu, A.; Ho, R. Y. N.; Que, L. J.; Ryle, M. J.; Phinney, B. S.; Hausinger, R. P. Alternative Reactivity of an A-Ketoglutarate-Dependent iron(II) Oxygenase: Enzyme Self-Hydroxylation. *J. Am. Chem. Soc* **2001**, 123, 5126–5127. DOI: 10.1021/ja005879x.

155. Sabourin, P. J.; Bieber, L. L. The Mechanism of α-Ketoisocaproate Oxygenase: Formation of β-hydroxyisovalerate from α-ketoisocaproate. *J. Biol. Chem.* **1982**, 257, 7468–7471.

156. Baldwin, J. E.; Adlington, R. M.; Crouch, N. P.; Pereira, I. A. C. Incorporation of 18o-Labelled Water into Oxygenated Products Produced by the Enzyme Deacetoxy/Deacetylcephalosporin C Synthase. *Tetrahedron* **1993**, 49, 7499–7518. DOI: 10.1016/S0040-4020(01)87226-4.

157. Baldwin, J. E.; Adlington, R. M.; Crouch, N. P.; Pereira, I. A. C.; Aplin, R. T.; Robinson, C. Water Exchange of Intermediates in a Non-Haem Iron, α-ketoglutarate Dioxygenase, Deacetoxy-/Deacetylcephalosporin C Synthase. *J. Chem. Soc., Chem. Commun.* **1993**, 105–108. doi:10.1039/C39930000105.

158. Baldwin, J. E.; Adlington, R. M.; Schofield, C. J.; Sobey, W. J.; Wood, M. E. The Role of α-ketoglutarate in Cephalosporin Biosynthesis. *J. Chem. Soc., Chem. Commun.* **1989**, 1012–1015. doi:10.1039/C39890001012.

159. Groves, J. T.; Haushalter, R. C.; Nakamura, M.; Nemo, T. E.; Evans, B. J. High-Valent Iron-Porphyrin Complexes Related to Peroxidase and Cytochrome P-450. *J. Am. Chem. Soc.* **1981**, 103, 2884–2886. DOI: 10.1021/ja00400a075.

160. Bernadou, J.; Fabiano, A.-S.; Robert, A.; Meunier, B. "Redox Tautomerism" in High-Valent Metal-Oxo-Aquo Complexes. Origin of the Oxygen Atom in Epoxidation Reactions Catalyzed by Water-Soluble Metalloporphyrins. *J. Am. Chem. Soc.* **1994**, 116, 9375–9376. DOI: 10.1021/ja00099a083.

161. Lee, K. A.; Nam, W. Determination of Reactive Intermediates in Iron Porphyrin Complex-Catalyzed Oxygenations of Hydrocarbons Using Isotopically Labeled Water: Mechanistic Insights. *J. Am. Chem. Soc.* **1997**, 119, 1916–1922. DOI: 10.1021/ja9629118.

162. Bernadou, J.; Meunier, B. "Oxo-Hydroxo Tautomerism" as Useful Mechanistic Tool in Oxygenation Reactions Catalysed by Water-Soluble Metalloporphyrins. *Chem. Commun.* **1998**, 1, 2167–2173. DOI: 10.1039/a802734j.

163. Puri, M.; Company, A.; Sabenya, G.; Costas, M.; Que, L. Oxygen Atom Exchange between H2O and Non-Heme Oxoiron(IV) Complexes: Ligand Dependence and Mechanism. *Inorg. Chem.* **2016**, 55, 5818–5827. DOI: 10.1021/acs.inorgchem.6b00023.

164. Flashman, E.; Hoffart, L. M.; Hamed, R. B.; Bollinger, J. M.; Krebs, C.; Schofield, C. J. Evidence for the Slow Reaction of Hypoxia-Inducible Factor Prolyl Hydroxylase 2 with Oxygen. *FEBS J.* **2010**, 277, 4089–4099. DOI: 10.1111/j.1742-4658.2010.07804.x.

Q17